NPS-67-84-021PR

NAVAL POSTGRADUATE SCHOOL

Monterey, California

SUBSONIC CASCADE WIND TUNNEL TESTS OF A SUNDSTRAND CONTOLLED-DIFFUSION FAN BLADE SECTION

A.G. McGuire and R.P. Shreeve

December 1984

Prepared for: Sundstrand Aviation Operations
Rockford, Illinois

NAVAL POSTGRADUATE SCHOOL

Monterey, California

Rear Admiral R. H. Shumaker
Superintendent

D. A. Schrady
Provost

This report formally documents the results and conclusions of a cascade wind tunnel test program sponsored by Sundstrand Aviation Operations, Sundstrand Corporation, (Purchase Order No. B2E4745-24M, dated 9/20/82) under the cognizance of Dr. Paul Hermann.

This report was prepared by

SECURITY CLASSIFICATION OF THIS PAGE *(When Data Entered)*

REPORT DOCUMENTATION PAGE

READ INSTRUCTIONS BEFORE COMPLETING FORM

1. REPORT NUMBER: NPS67-84-021PR	2. GOVT ACCESSION NO.
3. RECIPIENT'S CATALOG NUMBER	
4. TITLE *(and Subtitle)*: SUBSONIC CASCADE WIND TUNNEL TESTS OF A SUNDSTRAND CONTROLLED-DIFFUSION FAN BLADE SECTION.	5. TYPE OF REPORT & PERIOD COVERED: Final Report SEPT 1982-SEPT 1984
	6. PERFORMING ORG. REPORT NUMBER
7. AUTHOR(s): A. G. McGuire & R. P. Shreeve	8. CONTRACT OR GRANT NUMBER(s): P.O. No.B2E4745-24M Doc. No. N6277183WE30005
9. PERFORMING ORGANIZATION NAME AND ADDRESS: Naval Postgraduate School Monterey, California 93943	10. PROGRAM ELEMENT, PROJECT, TASK AREA & WORK UNIT NUMBERS
11. CONTROLLING OFFICE NAME AND ADDRESS: SUNDSTRAND AVIATION OPERATIONS 4747 Harrison Avenue Rockford, Illinois 61101	12. REPORT DATE: December 1984
	13. NUMBER OF PAGES: 59
14. MONITORING AGENCY NAME & ADDRESS *(if different from Controlling Office)*: Naval Postgraduate School Monterey, California 93940	15. SECURITY CLASS. *(of this report)*
	15a. DECLASSIFICATION/DOWNGRADING SCHEDULE

16. DISTRIBUTION STATEMENT *(of this Report)*

17. DISTRIBUTION STATEMENT *(of the abstract entered in Block 20, if different from Report)*

18. SUPPLEMENTARY NOTES

19. KEY WORDS *(Continue on reverse side if necessary and identify by block number)*
Controlled diffusion
Fan blade design
Cascade wind tunnel

20. ABSTRACT *(Continue on reverse side if necessary and identify by block number)*
Results are given of subsonic Cascade wind tunnel tests of a controlled diffusion fan blade section designed by Sundstrand Corporation. Data were obtained successfully at air inlet angles less than and approaching design incidence. Operation at design and higher incidence angles would require side wall suction. It was concluded that the design was successful and that a fan test should be considered.

DD FORM 1 JAN 73 1473 EDITION OF 1 NOV 65 IS OBSOLETE
S/N 0102-014-6601

SECURITY CLASSIFICATION OF THIS PAGE *(When Data Entered)*

Table of Contents

LIST OF TABLES

List of Figures

I. INTRODUCTION

Sundstrand's interest in "controlled-diffusion" (CD) blading was expressed in early 1982. The Turbopropulsion Laboratory was then engaged in an experimental program to evaluate CD blading designed by NASA in a 60" X 10" Subsonic Cascade Wind Tunnel. The Laboratory responded in July 1982 to a request for a similar test program to be conducted on a Sundstrand CD blading design. Initial funding to proceed was received 20 September 1982 for a program estimated to require on year to complete. Following receipt of blading coordinates and one revision, blading was designed procured and tested. The useful data obtained and the limitations experienced in the range of test parameters which could be simulated were transmitted to Sundstrand in September 1984. The present report documents the results and conclusions of the test program to that date.

The Sundstrand CD cascade design represented a more severe experimental challenge than had the NASA CD blading reported in Ref. 1. Diffusion factors were to be near 0.6 at air inlet angles close to 70° whereas the NASA design was for less than 0.4 at about 40° inlet air angle. As was the case for the NASA blades, considerable time was spent in trying to obtain acceptably uniform inlet and periodic outlet flow conditions before data were collected. Geometrical changes to the facility itself were experimentally evaluated before the static pressure distributions ahead of the blading were understood and accepted.

Unfortunately, air inlet angles of 70° (and, it was assumed, larger) gave rise to unstable flow conditions. This does not mean that the blade itself was designed to stall at these conditions, but rather that the corner flows, fed by the thick sidewall boundary layers, triggered a propagating stall

condition in the 3-dimensional geometry. Suction through the sidewalls throughout the blade passage is required in order to overcome this limitation. While such a modification is now planned the heavy steel construction of the facility would not permit even an improvised suction scheme for the present tests. The data obtained and presented here are therefore at negative incidence angles with respect to the design condition. The data are considered meaningful as part of an overall program to evaluate CD blading in the fan designs. The difficulties encountered in generating controlled 2D inlet conditions at very high inlet air angles lead to a recommendation that a complete fan should be built and tested.

II. TEST FACILITIES AND INSTRUMENTATION

A. Cascade Facility

The cascade facility is shown schematically in Fig. 1. The air supply is a 700 HP blower located in the basement. A conical screen and plenum turning vanes generate nearly uniform flow at low turbulence levels into the inlet guide vanes. The guide (or turning) vanes are adjustable to allow matching of the IGV exit flow angle to the angle setting of the lower walls.

The cascade wind tunnel geometry is shown if Fig. 2. The test section is 10" x 60" and can be supplied at air inlet angles, β_1, of up to approximately 75° measured from the verticle. The cascade geometry for the present test is shown in Fig 3. Blade spacing was 3 inches. The cascade was operated at Reynolds numbers of approximately 5×10^5, and Mach number of approximately 0.23.

B. Instrumentation

Two types of probes were used in the present tests. First, a rake probe was used to determine flow quality. As shown in Fig.4, the rake consists of 16 tubes; 15 sensors. The centermost sensor, consisting of two tubes detects yaw angle. At three and seven inches from the ends are static pressure sensors, and the remaining 12 are total pressure sensors.

Second, a United Sensor DA-125 5-hole probe, shown in Fig. 5, was used for detailed flow measurements alternately upstream and downstream of the test blading. Data were taken using a Hewlett-Packard 3052 Data Aquisition System and two 48 port Scanivalves.

Flow visualization included china clay, tufts, surface oils, and liquid soap bubbles.

C. Test Blading

The test blades were machined from 7075-T6 aluminum to the coordinates shown in Table I. The blade profile is shown in Fig 6. Three blades were instrumented with pressure taps at the locations shown in Table II. The central blade in the cascade had 36 taps, one at the leading edge, 20 distributed over the section surface and 15 over the pressure surface. The adjacent two blades had 6 taps each, 3 on the pressure side and 3 on the suction side. Two blades were black-anodized for flow visualization purposes. Nominal dimensions of the blades were 10" span and 4.02" chord.

III. EXPERIMENTAL PROCEDURE

A. General Procedure

Prior to acquiring data, several tests were performed to determine the procedures to be followed to adjust the cascade. These procedures were then followed routinely at each air inlet angle.

The cascade was initially configured to the geometrical parameters shown in Table III, but with the walls set for an air inlet angle of 70°. It was found that the cascade would not operate in a stable manner, and appeared to be stalled. Adjustments to the tail boards and IGV's failed to stablilize the flow. Lower values of air inlet angles of 62°, 64°, 68° were then attempted.

At each air inlet angle, the general procedure was to first survey the flow upstream and downstream of the test section using the rake probe. The 5-hole probe was then mounted and survey data were taken at the upper and then the lower survey plane. Surface pressures were then recorded. Flow visualization techniques were applied at various times, interspersed with the performance measurements.

B. Specific Procedures

1. Cascade Adjustments.

With the side wall removed, the inlet angle to the test section, β_1, was set by moving the lower end walls to the desired angle and clamping them in place. The IGV's were adjusted to align the trailing edge suction surface angle with the lower walls to approximate the flow streamline through a blade passage. The upper walls were set to the estimated exit flow angle, β_2, and the steel side wall was set in place.

The cascade was turned on and coordinated adjustments were made to the upper end walls and the inlet guide vanes. Both adjustments were made while

viewing the wall static pressure distributions on water-column manometers. When upper and lower wall static pressures were as uniform as the adjustments would allow, the cascade was considered to be ready.

2. Rake Probe Surveys

The rake probe surveys were carried out to verify the uniformity and periodicity of the flow. Measurements were obtained over 20" in the blade-to-blade direction, centered about the cascade centerline. At 1" intervals, the flow angle, total, and static pressures were recorded. This procedure was followed with the rake probe mounted in turn at the lower and upper measuring planes. The survey results were examined and the uniformity and periodicity were verified before proceeding further.

3. 5-hole Probe Surveys

5-hole probe surveys were also carried out in turn with the probe mounted at the lower and upper survey planes. At each plane, measurements were made in the spanwise and in the blade-to-blade direction, at 1/4" intervals. The blade-to-blade measurements covered a distance of 6 inches on either side of the spanwise centerline. Probe pressure data were recorded and stored with cascade reference data for off-line reduction and analysis.

4. Blade Surface Pressures

Blade surface pressures were recorded with cascade reference data following the 5-hole probe surveys.

5. Data Reduction

The data were reduced using procedures and programs developed by Cina (Ref. 2) and later modified by Himes (Ref. 3). A flowchart showing the acquisition and reduction sequence is shown in Fig. 7.

6. Flow Visualization

Surface flow visualization included: 1) surface oil, 2) china clay, 3) tufts, and 4) liquid soap film. The china clay method was discontinued during the program because of operational difficulties involved in controlling the application of the developer solution. Still photographs and movies were made of the other techniques at angles of 64° and 68°. In general, flow visualization was carried out in a separate test but without change in the cascade adjustments.

IV. RESULTS

A. Rake Surveys

The results of rake surveys taken over the center 20 inches of the cascade, in the blade-to-blade direction, at inlet wall settings of 68°, 64°, and 62°, are shown in Fig. 8, 9 and 10, respectively.

Part 'a' of each figure shows measurements from four total pressure sensors at ∓0.75 inches and ∓1.5 inches spanwise from the centerplane and two static pressure sensors at ∓2 inches from the center plane. The pressures were measured relative to atmospheric pressure and were made dimensionless by dividing by a reference dynamic pressure calculated from the cascade plenum (total) and lower wall (static) pressure.

Part 'b' of each figure shows the difference between the pressures in inches of water measured by the two tubes of a yaw-sensor at the center of the rake. A yaw angle of one degree corresponded to a pressure differential of approximately 3/4 inches of water.

B. Surface Flow

Visual observation of the surface flow was facilitated by tufts in two blade passages (between blades 5 & 6, and 13 & 14, respectively). Movies were taken of the tufts. No prints are included here since the observed time averaged behavior was illustrated best by oil-smear photographs.

Figures 11, 12 and 13 show photographs of oil smear patterns obtained at wall setting of 68°, 64° and 62°, respectively. Spots of various mixtures of materials were applied with a wand just before the flow was started. The material flowed and subsequently dried during steady operation. The blade was removed and photographed after the test.

Fig. 14 shows patterns formed on the window as a result of soap-bubble

solution bled through a single static pressure tap just ahead of the blade.

C. Blade Surface Pressures

Blade surface pressures were reduced to pressure coefficients using the average inlet static and average inlet dynamic pressures deduced from the survey probe data. The results are shown in Fig.15.

D. Probe Surveys

Data recorded from probe surveys at upstream and downstream planes were reduced to obain the loss coefficient, the area-averaged outlet flow angle and the axial-velocity density ratio (AVDR). The results are shown plotted as a function of the inlet air angle in Figs. 16, 17 and 18, respectively. The diffusion factor was calculated from the measured flow angles and the results are shown plotted in Fig.19. The AVDR is shown as a function of diffusion factor in Fig.20.

V. DISCUSSION

Discussion of the blade element performance measurements is prefaced by a discussion of the flow conditions under which they were obtained.

A. Inlet Flow Quality

Data were taken after adjustments were made to the IGV's and outlet tailboards. The settings chosen for these adjustments were selected on the basis of the blade-to-blade static pressure distributions observed on the water column manometer board. The degree to which uniformity of the inlet flow field was achieved can be judged from the rake data shown in Figs.8-10. The results showed the following:

1. The total pressure was uniform to within measurement accuracy over the center 3 inches in the spanwise direction.
2. The total pressure varied $\mp 2\%$ of the reference dynamic pressure in the blade-to-blade direction at $\beta i_w = 64^\circ$, and less at larger values of βi_w, due to wakes of the IGV's.
3. The static pressure varied approximately 0.5% of the reference dynamic pressure per blade space in the blade-to-blade direction at $\beta i_w = 68^\circ$ and less at the smaller values of βi_w.
4. The measured flow angle was uniform to within 0.5 degree over the most central 5 blade passages. It was noted that the air inlet angle ($\beta 1$) departed from the wall setting (βi_w) by 0.5° to 1.1°.

Thus the inlet flow angle was uniform about the center plane, to within acceptable limits.

B. Three Dimensional Effects

In the absence of suction, non-planar flow effects were inevitably

present which gave rise to an AVDR greater than one and three-dimensional viscous effects in the blade-end wall junctions. The oil-smear records in Figs.11-13 show clearly the extent of non-planar surface effects at the ends of the blades. Also, the liquid soap-film technique (Fig.14) showed the presence of separation and vortex motion on the end walls. The center of the blade span however always showed surface streamlines which, when attached, were parallel to the center plane. It was also verified by spanwise probe surveys that a 'core' of at least 2 inches persisted at the outlet measurement plane. The results obtained are therefore characteristic of a flow with stream surface contraction to the measured values of AVDR. The distribution of AVDR between the measurement stations is not known.

The following discussion refers to the flow at the mid-span section.

C. Pressure Distribution and Surface Flow

The measured surface pressure distributions shown in Fig. 15 suggest that the design air inlet angle was larger than 68°. Only at 68° did the peak Mach number over the blade suction surface become comparable to that over the pressure surface, although it was still smaller.

Toward the trailing edge, a significant loading is maintained. (A probable error in one pressure tap at 68° is indicated by a broken line). There is first an acceleration and then a deceleration over the final curvature on the suction side. The flow accelerates to the trailing edge on the pressure side.

No qualitative changes occured between the conditions at $\beta i_w = 62°$ and 64° (which gave air angles of 63.1 and 64.5). It was observed from both tufts and oil-smear that the flow was fully separated on the blade's pressure side (Fig.13). Forward flow at the oil spots close to the leading edge suggested

that a laminar separation occured there. In contrast, the surface streamlines apppeared to be attached and almost planar over the suction surface (Fig.13). Separation of the flow from the suction surface was indicated by the oil-smear to occur just downstream of the beginning of the trailing edge suction surface radius. Soap solution, injected through a wand near the trailing edge on the pressure side, flowed around the trailing edge and indicated the separation on the suction side. It is noted however that gravitational effects may have affected those observations to some degree. At $\beta i_w = 68^\circ$ ($\beta i = 68.4^\circ$), the pressure on the pressure side was increased and the distribution was smooth. Oil-smear indicated attached flow (Fig. 11).

The pressure distributions on both suction and pressure sides of the blade changed qualitatively at the highest inlet air angle. A more nearly constant pressure was developed on the pressure side and a more adverse gradient was developed on the suction side. An acceleration over the faired trailing edge was measured at all angles, notwithstanding the indication from flow visualization that separation occured at the beginning of the change in curvature.

D. Blade Performance

The loss coefficient, shown in Fig. 16, decreased from a value of almost 6% at air inlet angle of 63° to 3.6% at 68°. The data vary smoothly over the limited range of three angle settings which were tested. A fourth data point is shown at 65° air inlet angle. The fourth point was taken with perturbed settings of the IGV's and exit tail boards, giving static pressures at the east end of the cascade which were lower than at the west end and in the center, but with a very uniform distribution of inlet air angle. The departure of this point from the curve drawn through the other data is taken to indicate the maximum uncertainty resulting from judgement used in setting the cascade.

It is observed that the three data points may not be sufficient to define the loss variation properly. It is only at 68° that the flow remains attached on the pressure side of the blade. At 63° and 64 1/2°, a cavity-type separation was present. Also, the AVDR, shown in Fig.18 and Fig.20 changed dramatically in going to 68°. However, the corresponding increase in the diffusion factor shown in Fig.19 was almost linear.

An extremely unusual behavior was observed in the air outlet angle as the air inlet angle was increased. In terms of "deviation", the deviation angle decreased almost linearly when the air inlet angle was increased from 63° to 68°, corresponding to an increase in turning angle from 12° to 21°. It is only at the highest angle that the blading is producing the turning and diffusion intended in the design. It is seen in Fig. 21 that the changes measured in the flow angles are consistent with the changes in the direction of the blade force obtained by integrating the surface pressure distribution.

E. ANALYSIS

A finite element Code Q3DFLO-81 developed by Hirsch (Ref. 4), was applied to the Sundstrand cascade geometry, and predicted surface pressure coefficient distributions were compared with measured distributions. Data obtained in the preliminary test program at air inlet angles of 62° and 66° are shown in Fig. 22(a) and Fig. 22(b) respectively. Data obtained at 68° are shown in Fig. 23(a) and corresponding plots of the surface Mach Number, surface grid points, computational mesh and computed streamlines are shown in parts (b)-(e) of the same figure.

Several comments are offered. First, the data agree qualitatively with the computed results, but depart fairly significantly in magnitude. Second,

the inviscid prediction near the trailing edge on the suction side is not obtained in practice. As discussed above, there is an acceleration over the curved trailing edge, but it is much less than inviscid analysis would predict.

The departure of data and analysis in Fig. 22(a) at an air angle of 62° can be reasonably understood. The suction-side distribution agrees reasonably well except near the trailing edge where the flow was detected to separate. The measured distribution on the pressure side departs from the predicted distribution (and is thereafter flatter than predicted where the flow was observed to be fully separated).

It is observed in Fig. 22(b) that the surface pressures measured on both sides of the blade at an air angle of 66° are lower than predictions beyond about 20% of the chord. Unfortunately, no surface flow observations were made at this condition. The same is true however at an air inlet angle of 68° (Fig. 23(a)) at which the flow was found to be attached on both surfaces.

In all cases, the pressure levels near the trailing edge are lower than predicted by the code, which suggests that the measured static pressure rise across the cascade be examined. Under incompressible flow conditions, which is a reasonable approximation for the conditions of the tests, the static pressure rise coefficient can be shown to be given by

$$C_{p\ static} = 1 - (AVDR)^2 \frac{\cos^2\beta_1}{\cos^2\beta_2} + \bar{\omega} \qquad (1)$$

The following table compares the measured static pressure rise given in Table IV with that predicted by Eq. (1) using the measured values of AVDR, β_1, β_2 and $\bar{\omega}$. Also shown is the result of computing $C_{p\ static}$ using Eq. (1) with the measured β_1, β_2 and $\bar{\omega}$, but using AVDR = 1.

Measurements (Table IV)					C_p static (Eq. (1))	
β_1	β_2	AVDR	$\bar{\omega}$	$C_{pstatic}$	measured AVDR	AVDR = 1
68.4	47.1	1.486	.0364	.327	.391	.744
64.5	49.9	1.204	.0501	.312	.403	.603
63.1	51.1	1.188	.0585	.215	.326	.539

It is quite clear that the AVDR has a large effect on the static pressure rise across the cascade. It is also known from experience that the AVDR, and the distribution assumed for it through the computational domain, has a considerable effect on the surface pressure distribution which is computed. Thus it is tentatively concluded that the three-dimensional behavior through the blade passages, the value and axial distribution of the AVDR, is the cause of the differences between measurements and expectations.

VI. CONCLUSIONS

From the program of tests and analysis of the results, the following were concluded:

1. Useful data were obtained at incidence angles approaching and less than the design condition for the cascade.

2. Attached flow occured on both sides of the blading at the highest air inlet angle at which data could be obtained (68.4^{o}). The loss coefficient was measured to be 3.6% at a diffusion factor of 0.56 with an AVDR of 1.49.

3. By extrapolation of the data, from smaller angles, the minimum loss was indicated to occur at an air inlet angle of 70^{o} or greater. However propagating stall was encountered at these test conditions. The heavy steel construction of the facility would not allow control of the side wall boundary layers and corner flows which were the probable cause of stall.

4. The high diffusion factors gave rise to three dimensional effects in the blade passages which were not evident however, at the downstream plane where probe measurements were made.

5. The prediction of surface pressure distribution (and therefore incipient separation) requires a correct prescription of AVDR distribution and a modeling of the viscous behavior near the trailing edge.

6. In view of the demonstrated ability to design the CD contour, and the demonstrated difficulty associated with establishing well-controlled near-2D conditions in linear cascades at very large air inlet angles and diffusion factors, a concurrent test of a fan incorporating the present section should now be considered. Data from the fan test could then be compared with information which could be obtained in the cascade, with the development of wall boundary layer control during the same time frame.

TABLE I

Blade Surface Coordinates
(Inches - see Figure 6)

Suction Surface		Pressure Surface	
X	Y	X	Y
0.000	0.077	0.000	0.077
0.023	0.109	0.004	0.049
0.075	0.147	0.019	0.029
0.161	0.193	0.051	0.013
0.274	0.242	0.096	0.004
0.416	0.294	0.151	0.077
0.561	0.332	0.216	0.000
0.728	0.366	0.287	0.002
0.910	0.394	0.365	0.007
1.099	0.415	0.448	0.016
1.285	0.428	0.536	0.030
1.474	0.439	0.631	0.048
1.646	0.442	0.733	0.071
1.811	0.438	0.845	0.099
1.968	0.431	0.968	0.132
2.116	0.420	1.104	0.167
2.256	0.405	1.256	0.203
2.388	0.389	1.425	0.235
2.516	0.371	1.613	0.260
2.644	0.355	1.819	0.275
2.770	0.340	2.043	0.279
2.894	0.325	2.282	0.272
3.017	0.310	2.537	0.254
3.138	0.296	2.801	0.224
3.258	0.281	3.065	0.183
3.375	0.267	3.312	0.137
3.489	0.254	3.528	0.092
3.599	0.240	3.704	0.067
3.706	0.230	3.824	0.031
3.725	0.226	3.899	0.017
3.752	0.220	3.932	0.012
3.801	0.204	3.934	0.012
3.843	0.184	4.02	0.000
3.880	0.160		
3.913	0.134		
3.941	0.105		
3.967	0.075		
3.990	0.043		
4.011	0.010		
4.02	0.000		

TABLE II.

Pressure Tap Locations

Suction Side, (X)	Pressure Side, (X)
0.000	
0.051	0.085
0.135	0.190
0.225	0.315
0.330	0.480
0.480	0.660
0.675	0.925
0.925	1.170
1.170	1.420
1.425	1.730
1.685	2.055
1.885	2.375
2.185	2.690
2.515	3.190
2.900	3.705
3.335	3.840
3.520	
3.710	
3.810	
3.910	
3.975	

Table III

Test Parameters

chord, c	4.02
span, b	10.0
stagger angle, γ	58.24
spacing, s	3.0
solidity, σ	1.34
inlet air angle, β_1	62°-68°
outlet air angle, β_2	51°-47°

TABLE IV

Reduced Data

β_1	68.4°	64.5°	63.1°
β_2	47.1°	49.9°	51.1°
D	0.563	0.432	0.358
W	0.0364	0.0501	0.0585
AVDR	1.486	1.204	1.188
$C_{pstatic}$	0.327	0.312	0.215
C_{XM}	-.065	-.202	-.118 Tangential
C_{YM}	-.588	-.144	-1.052 Axial
C_{XB}	-.8697	-.8173	-.7337 Tangential
C_{YB}	-.507	-.2611	-.1390 Axial
Re	47730	55360	540290
$\Delta\beta$	21.3°	14.6°	12.0°

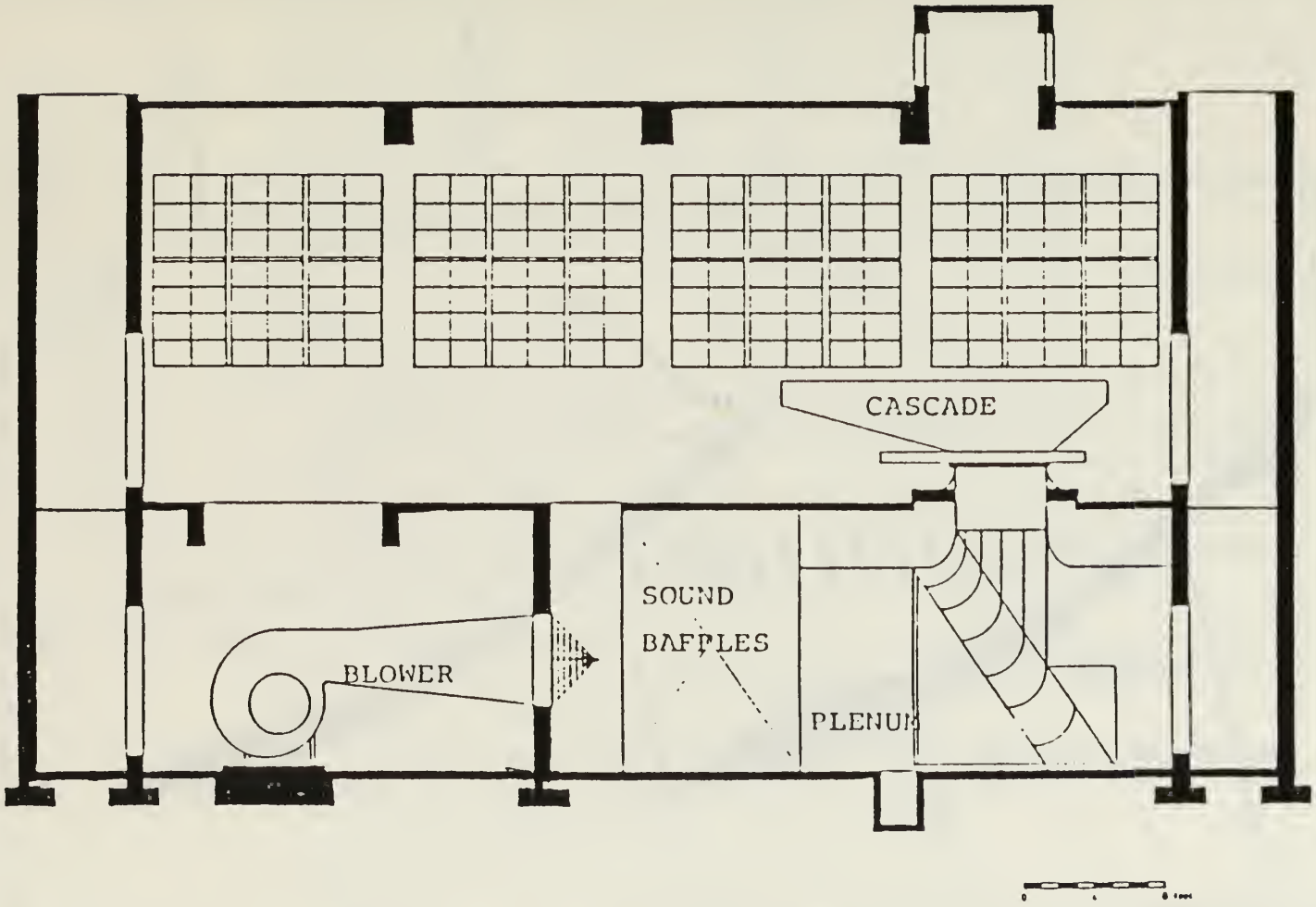

Figure 1. Cascade Wind Tunnel Test Facility.

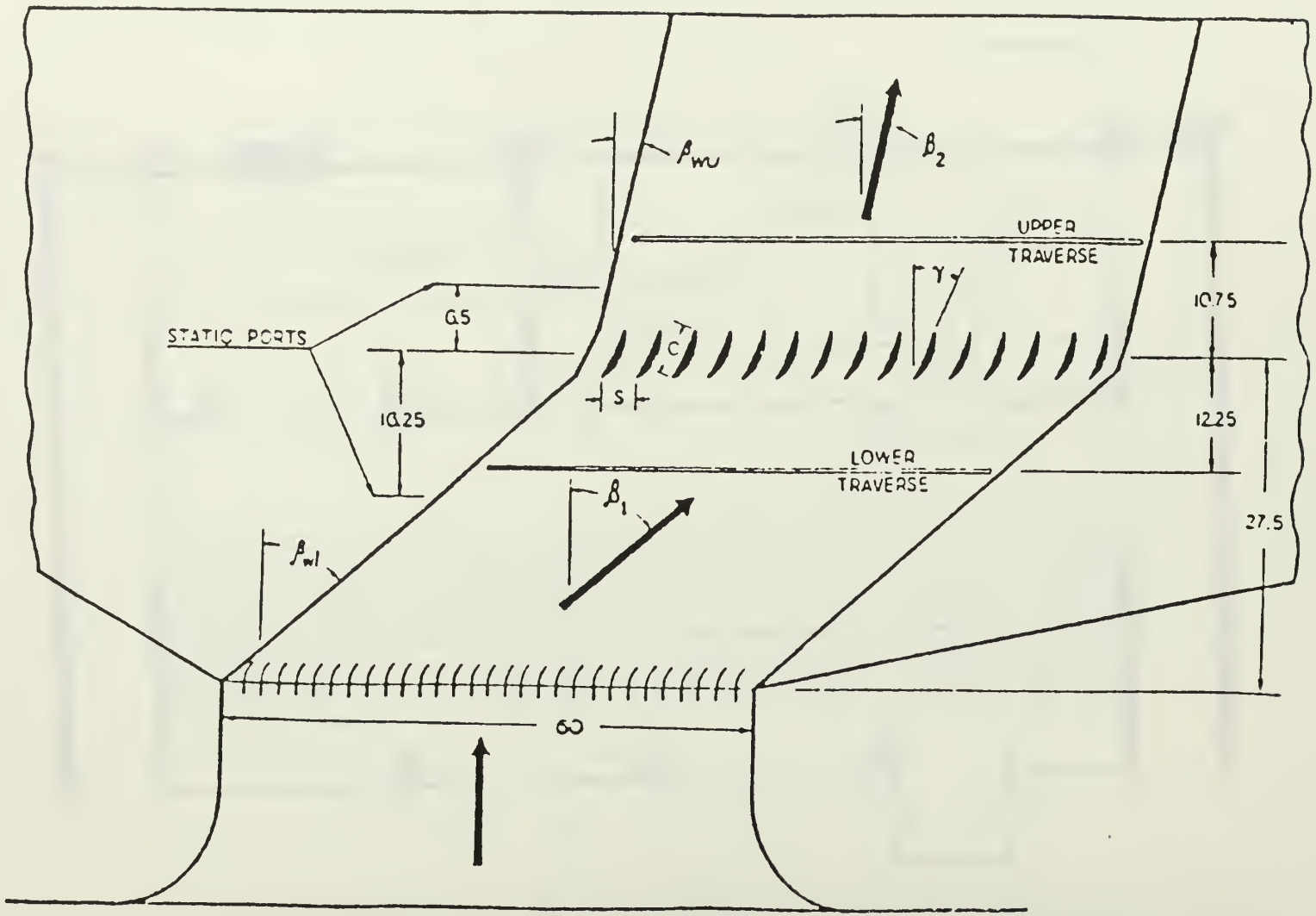

Figure 2. Cascade Test Section Schematic.

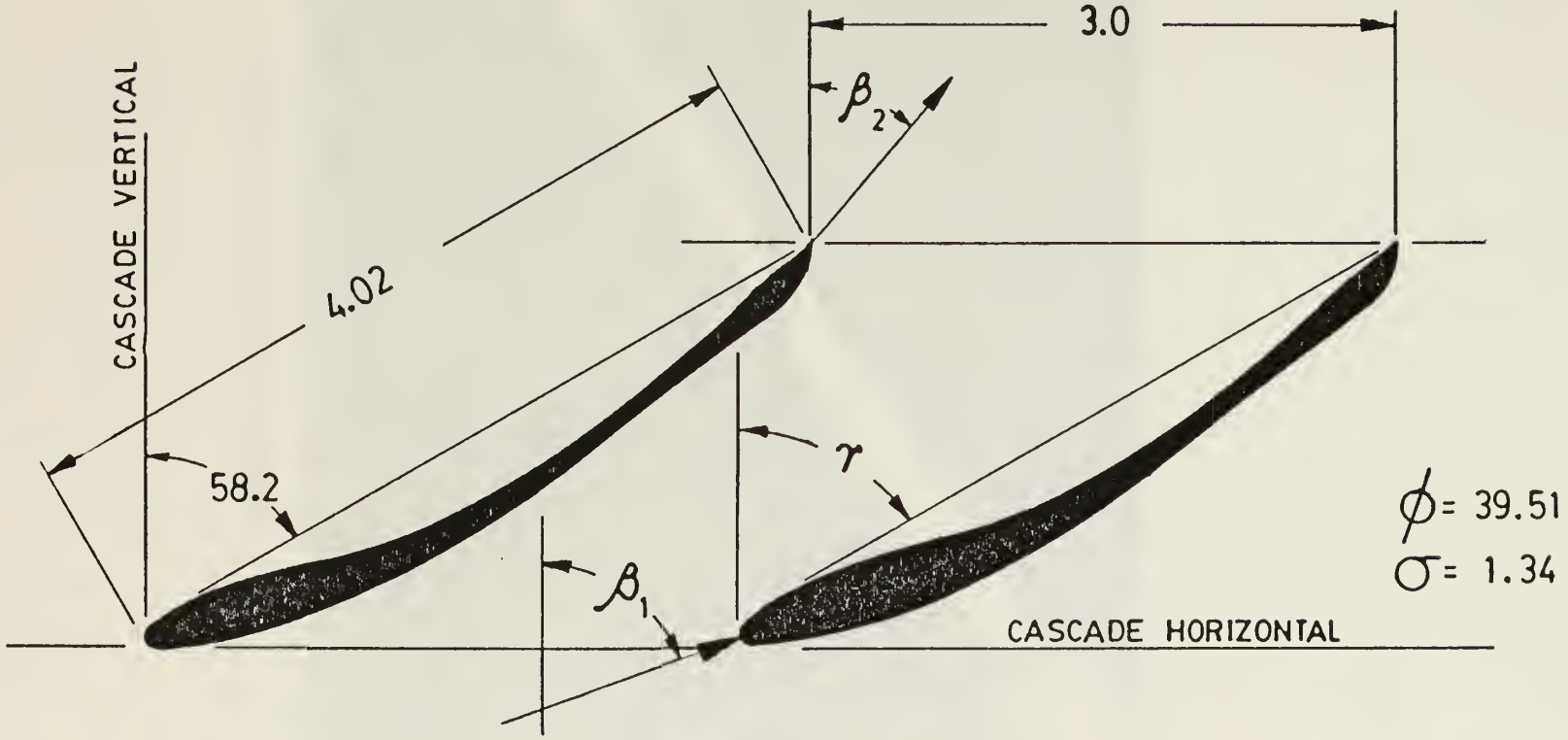

Figure 3. Sundstrand Blade Cascade Configuration.

Figure 4. Rake survey probe.

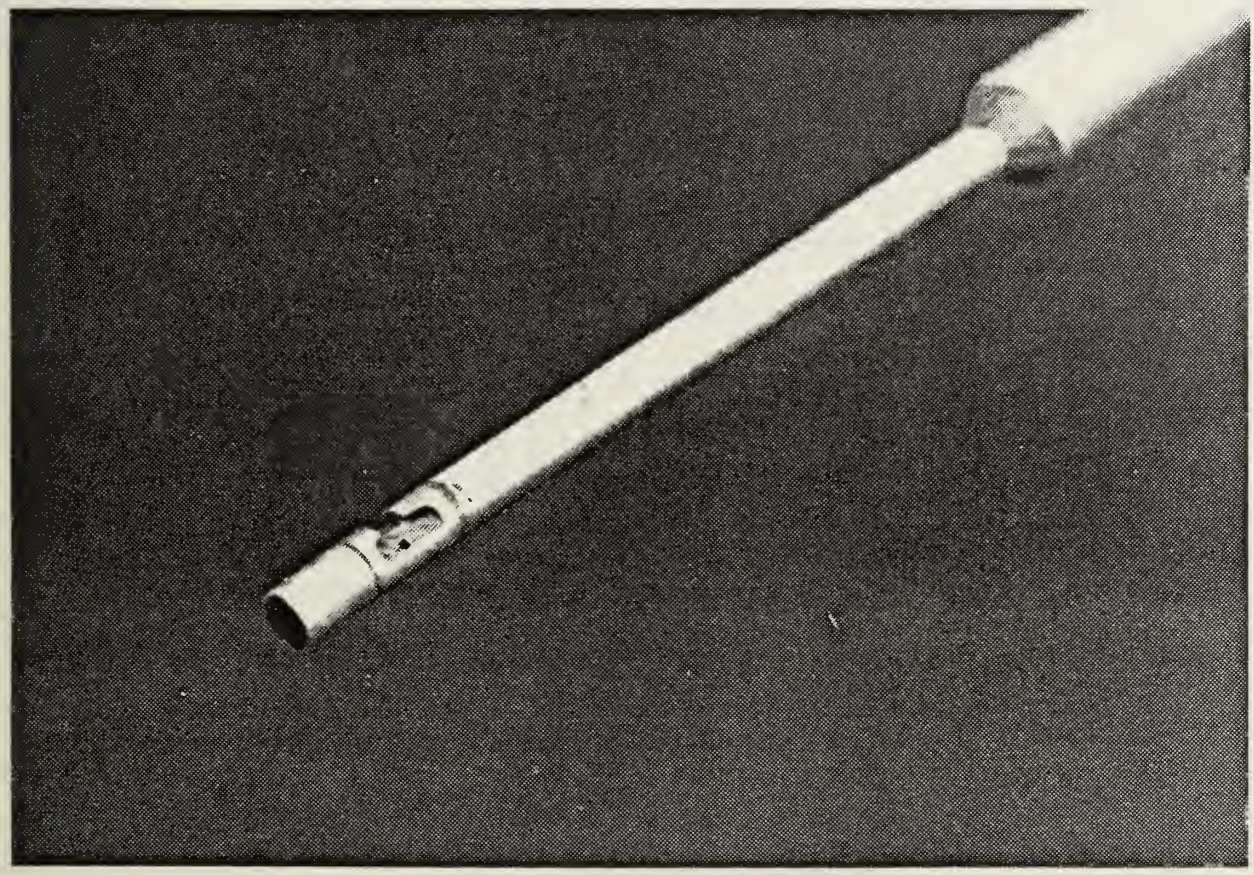

Figure 5. 5-hole Survey probe.

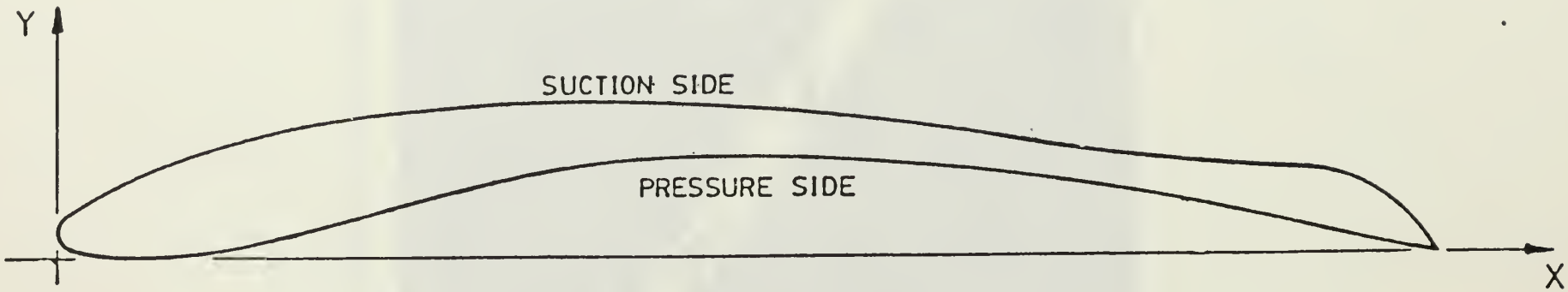

Figure 6. Blade Profile.

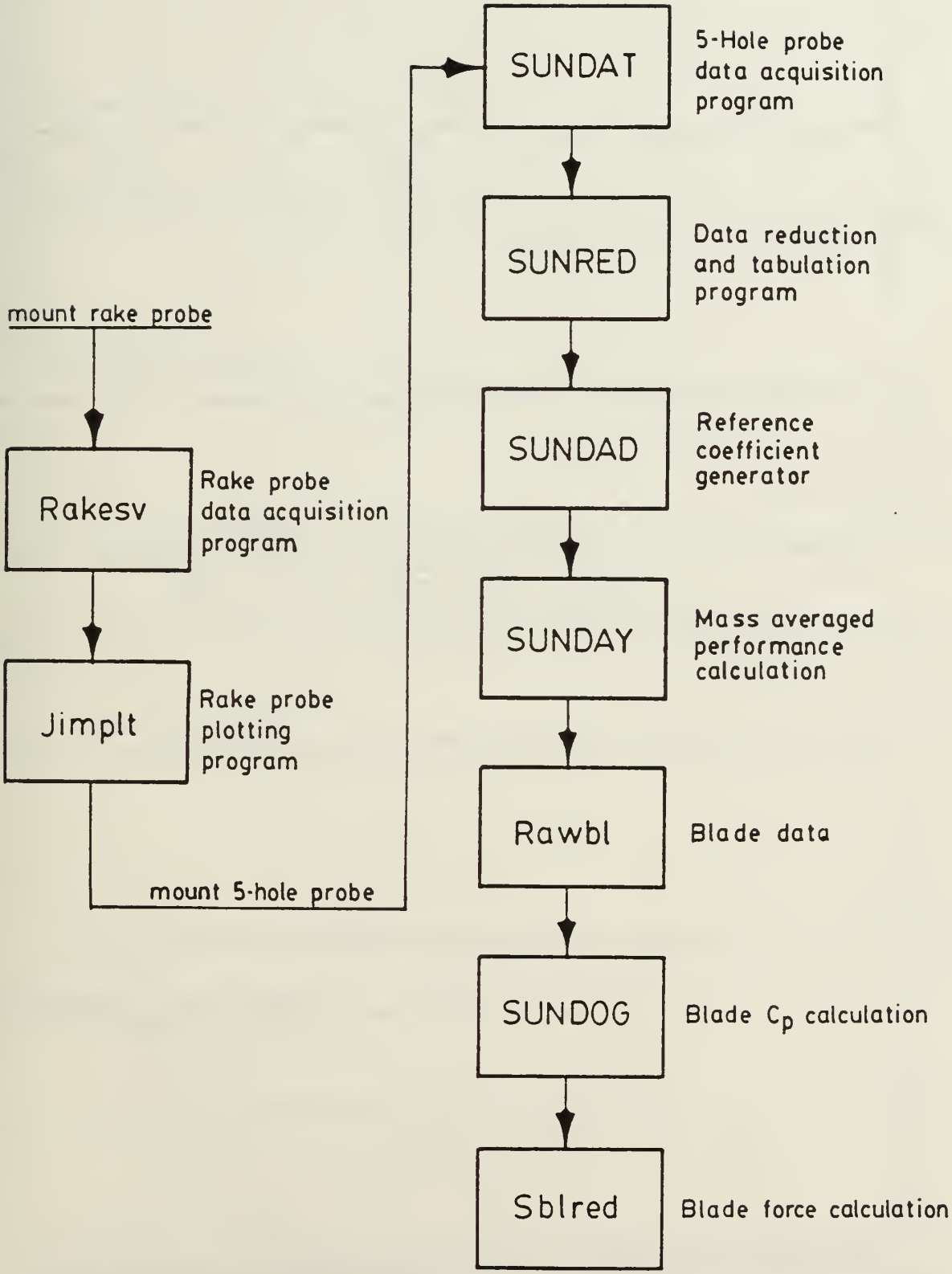

Figure 7. Flowchart of Data Acquisition and Reduction Software.

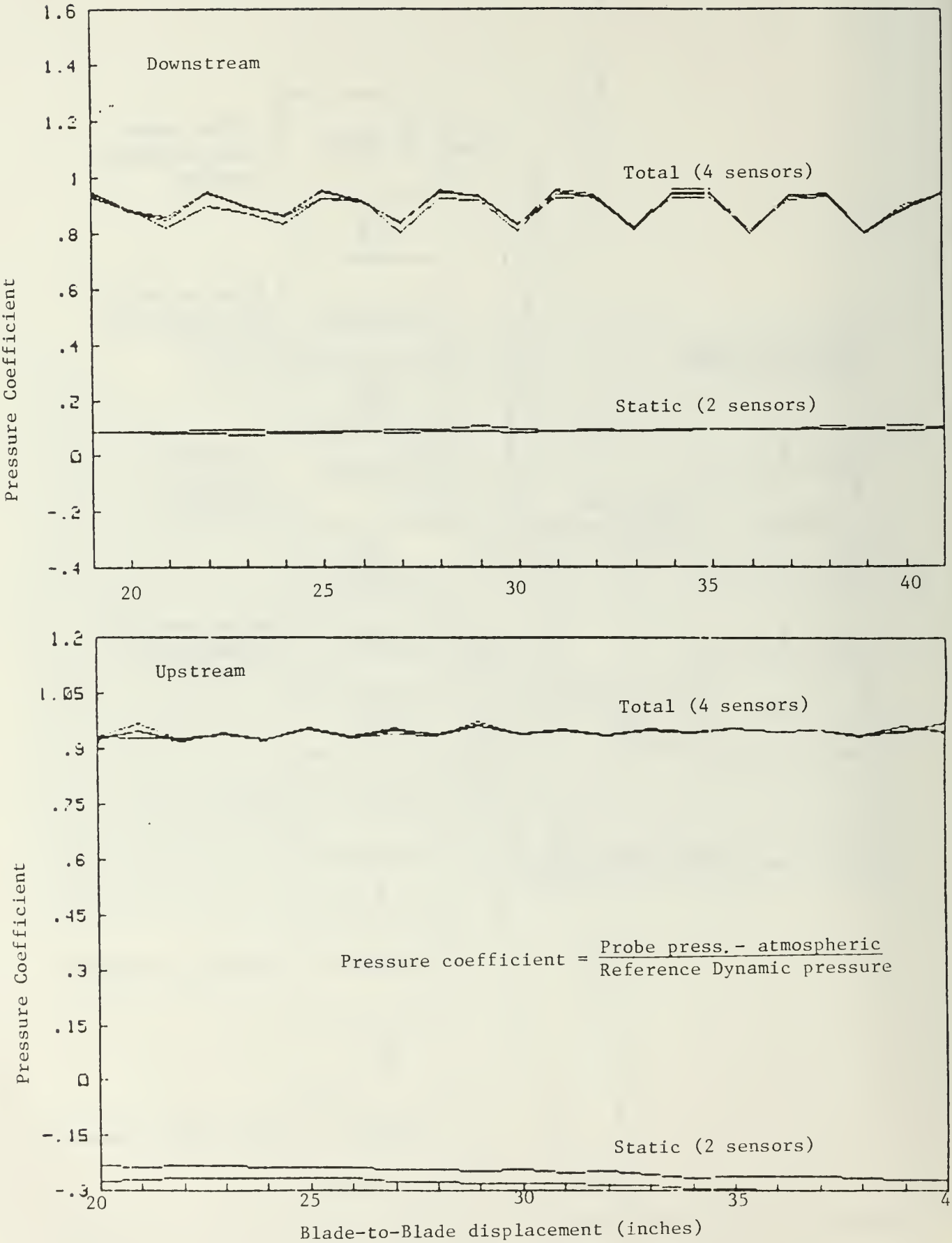

Figure 8a. Pressure Distribution Upstream and Downstream of the blading from Rake Surveys, $\beta_1 = 68^\circ$.

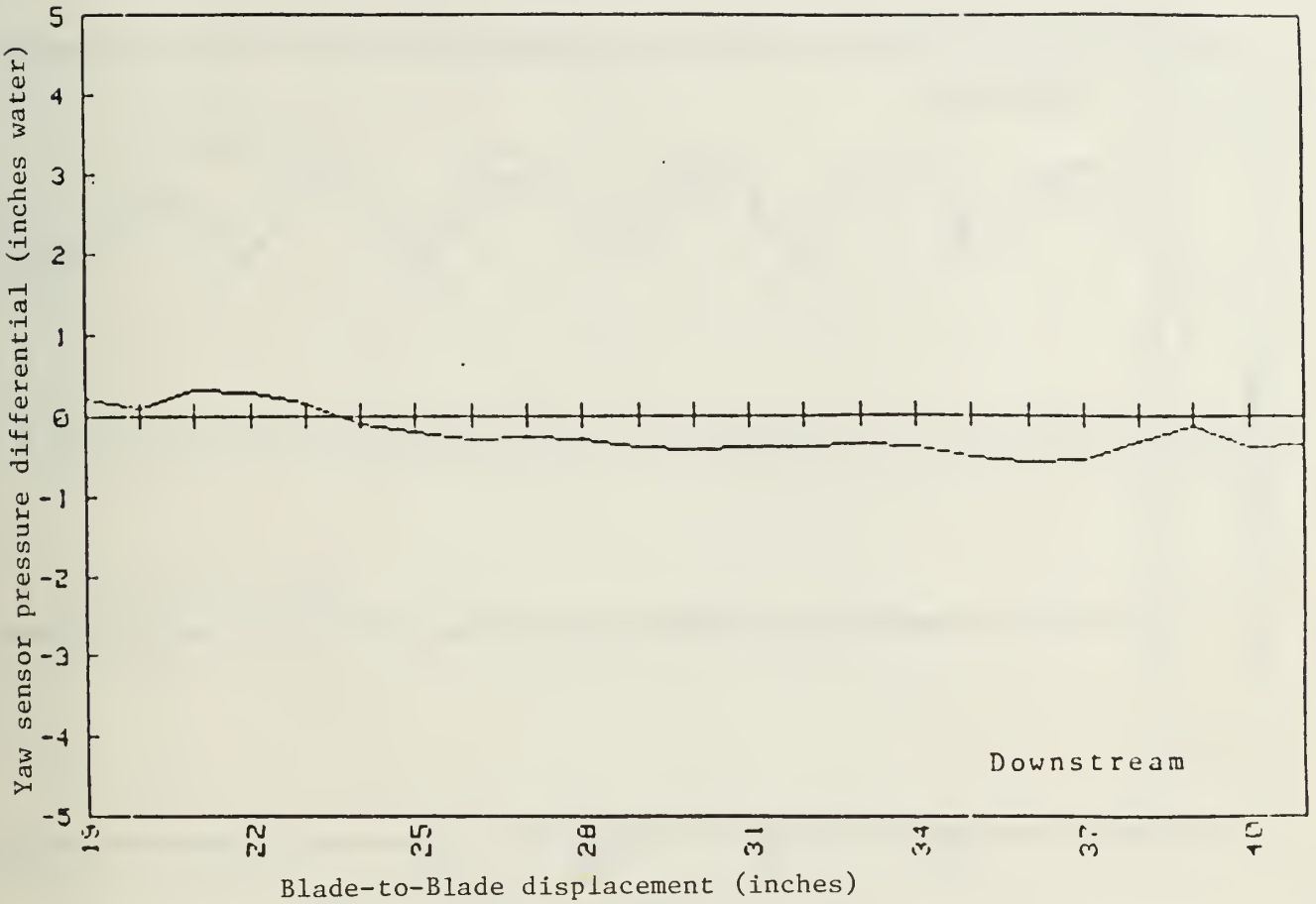

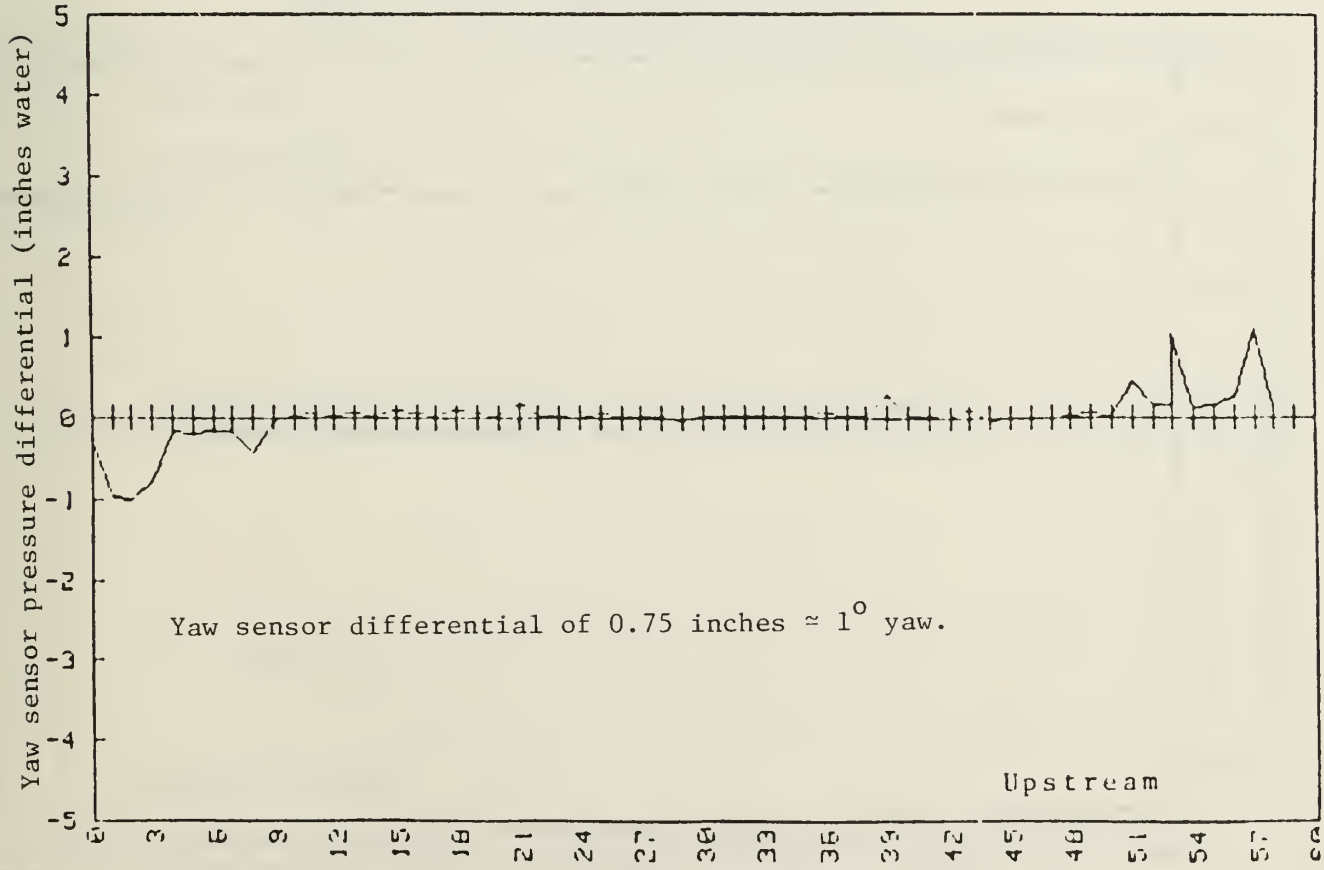

Figure 8b. Yaw Angle distribution upstream and downstream of the blading at $\beta_1 = 68^{\circ}$.

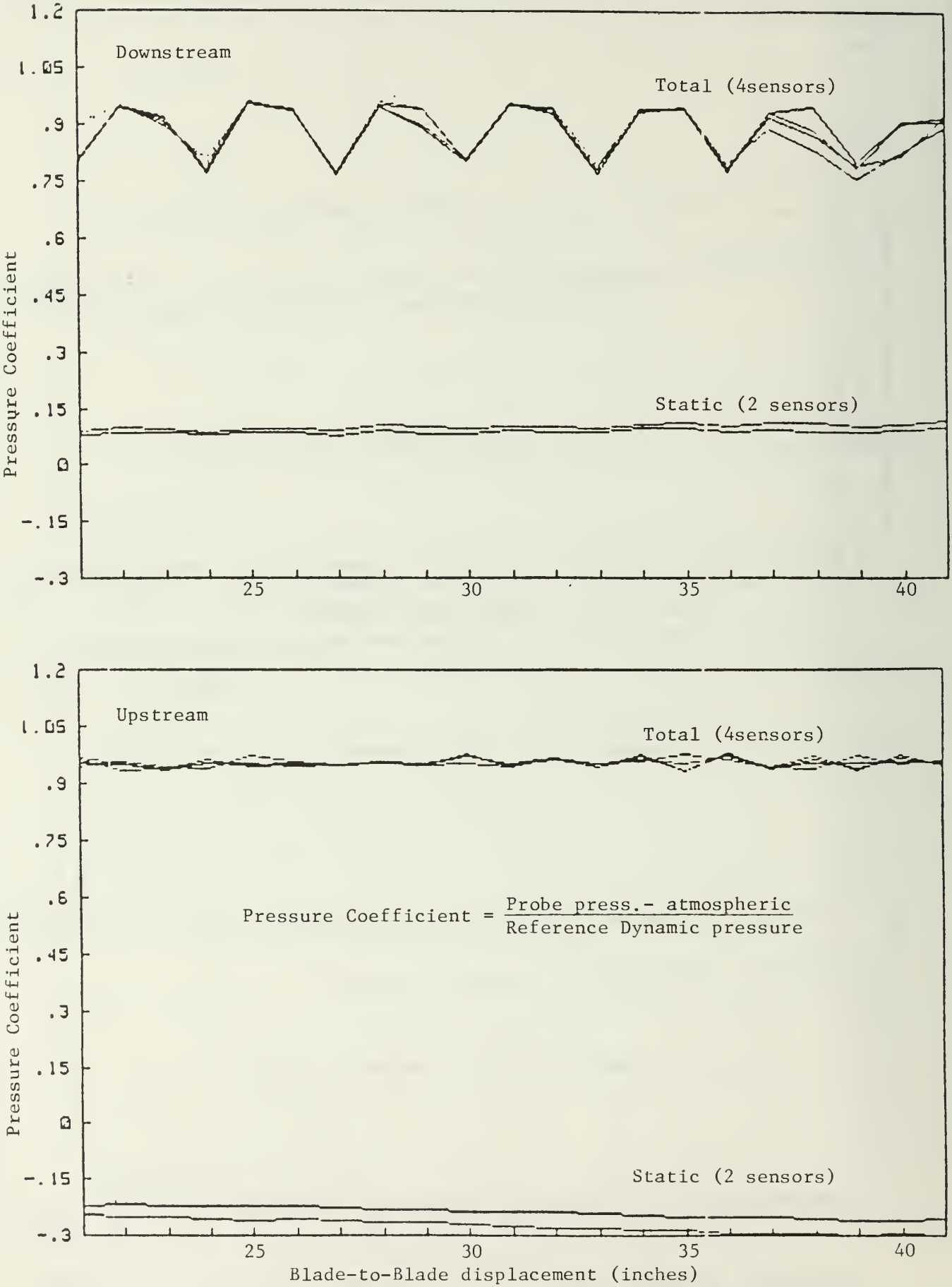

Figure 9a. Pressure distribution upstream and downstream of the blading from Rake Surveys, $\beta_1 = 64^\circ$.

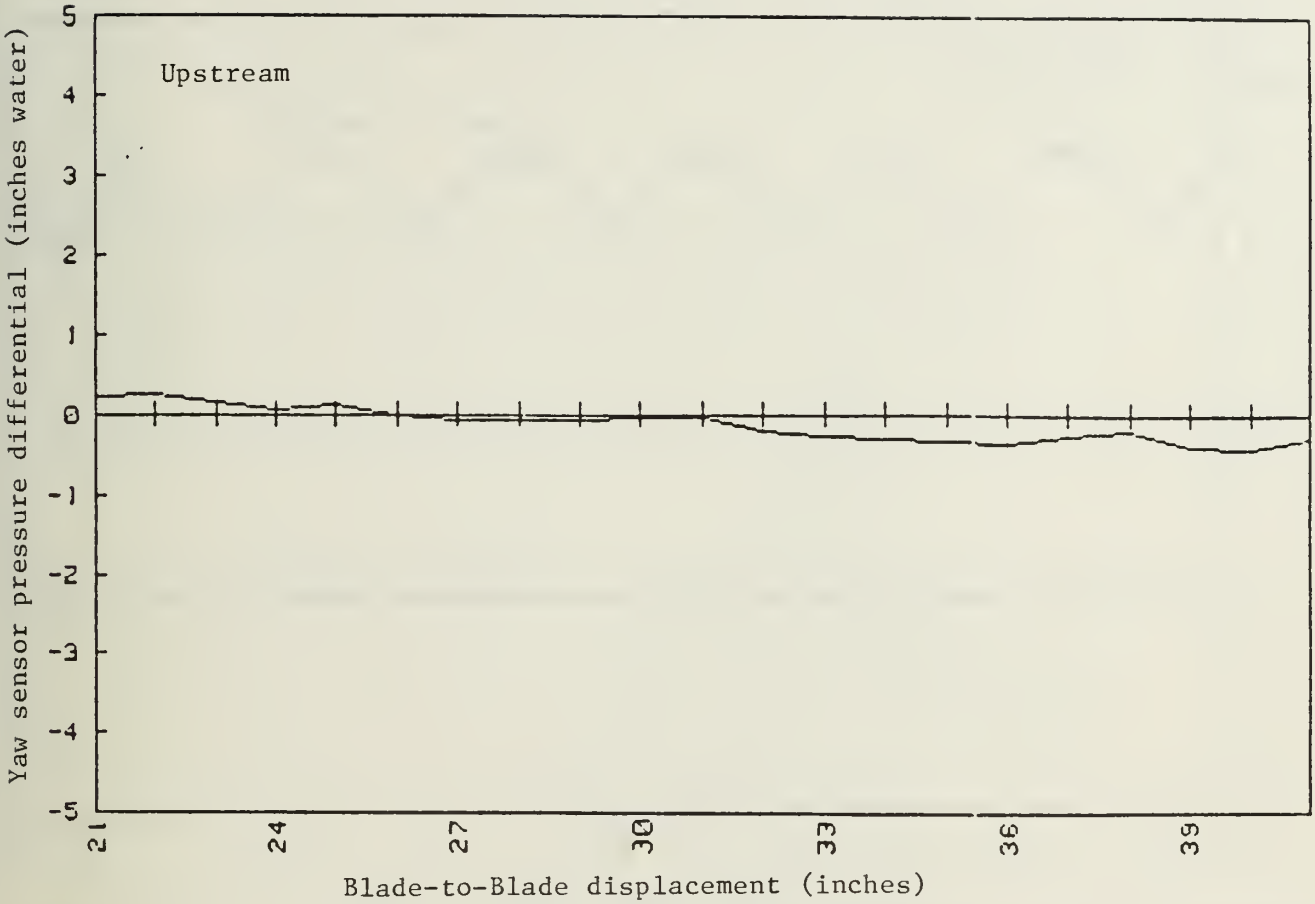

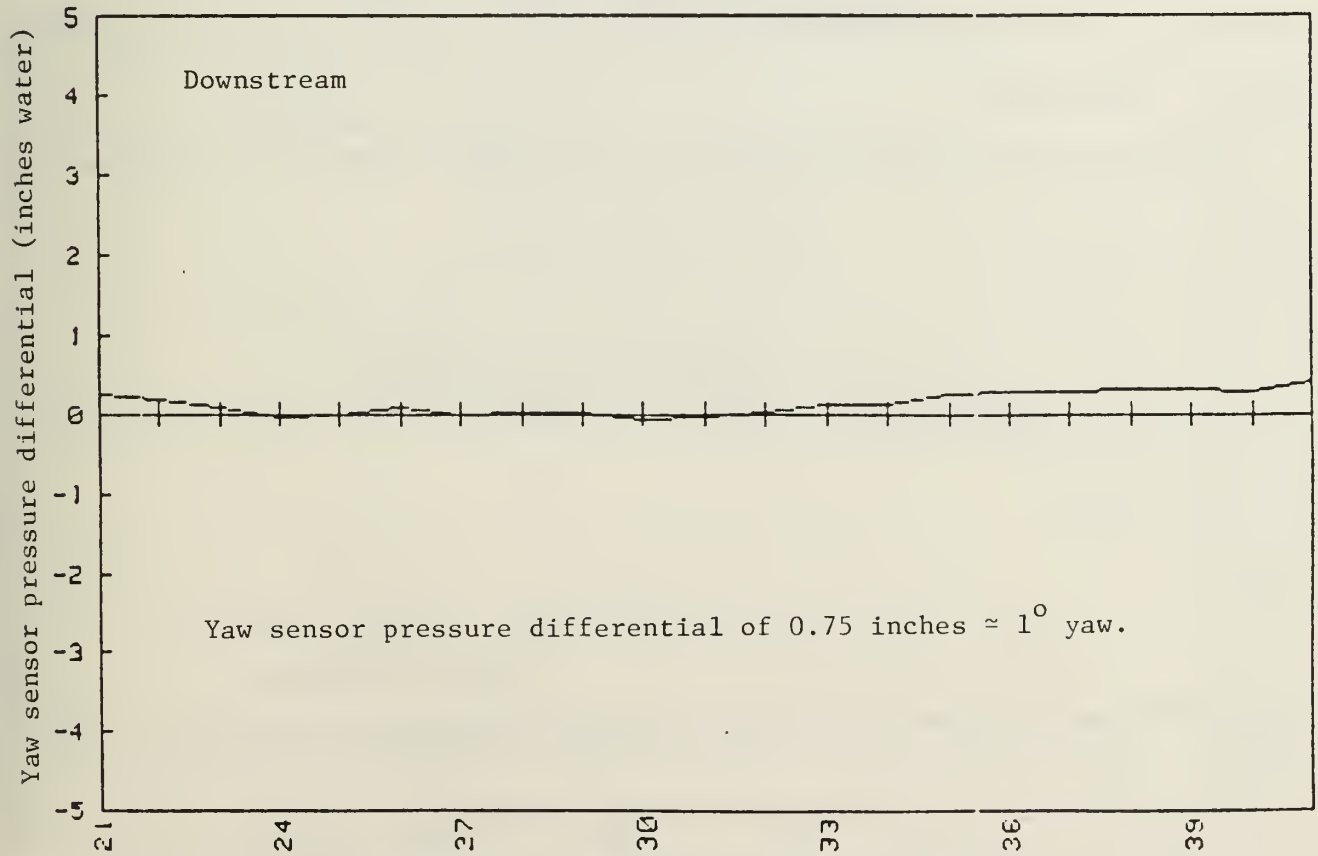

Figure 9b. Yaw Angle distribution upstream and downstream of the blading at $\beta_1 = 64^{\circ}$.

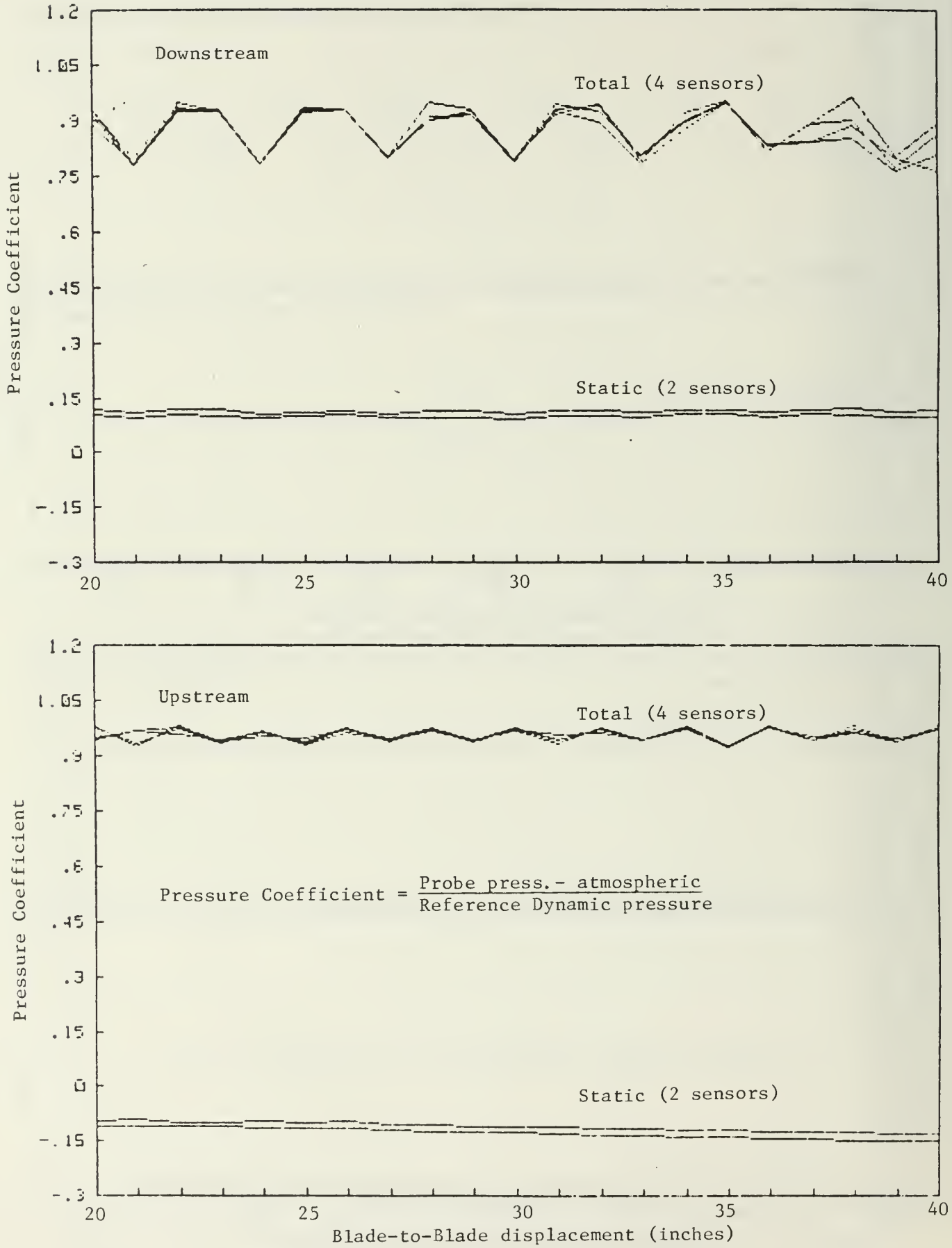

Figure 10a. Pressure distribution upstream and downstream of the blading from Rake Surveys, $\beta_i = 62^\circ$.

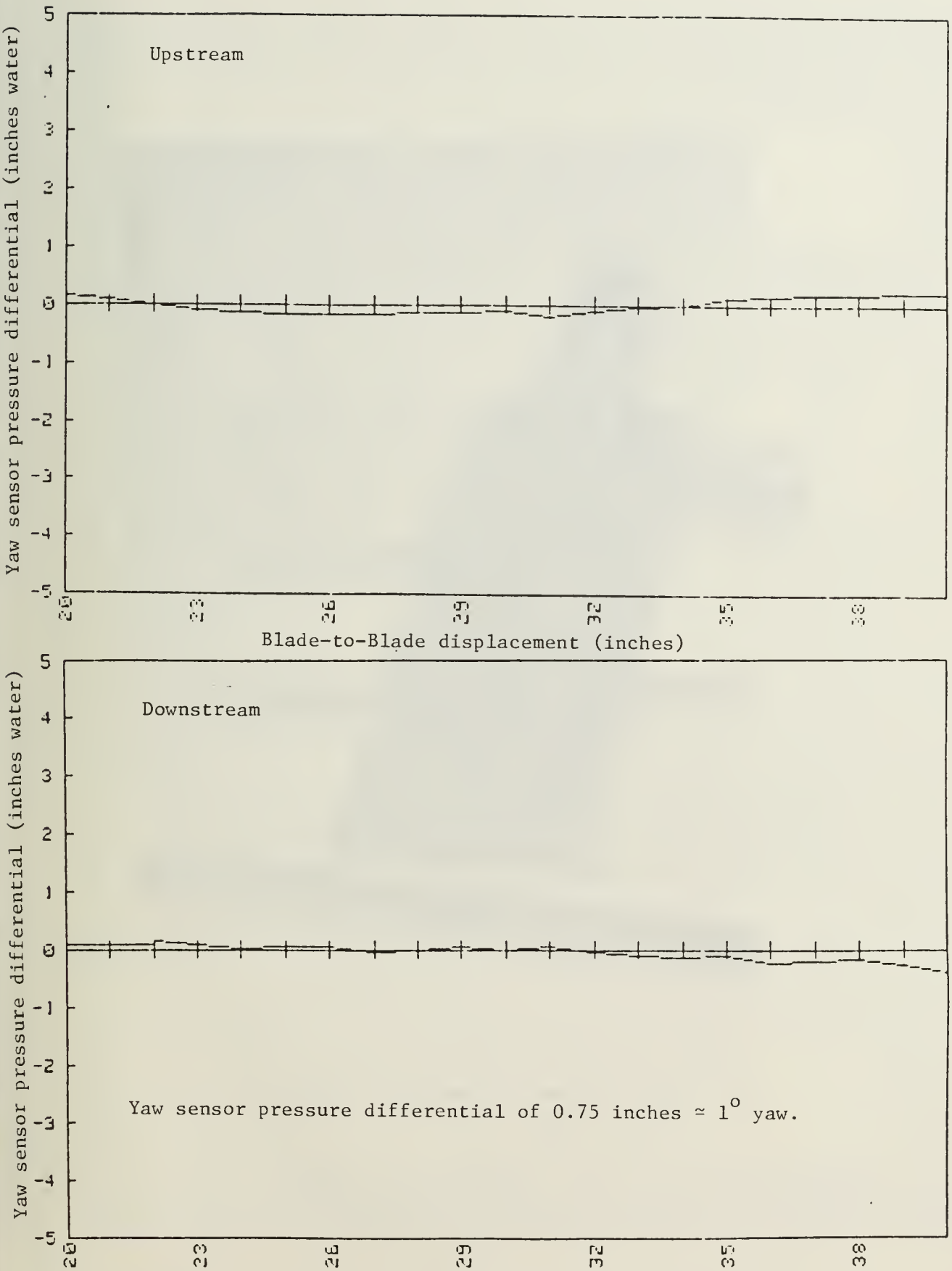

Figure 10b. Yaw angle distribution upstream and downstream of the blading at $\beta_1 = 62^{\circ}$.

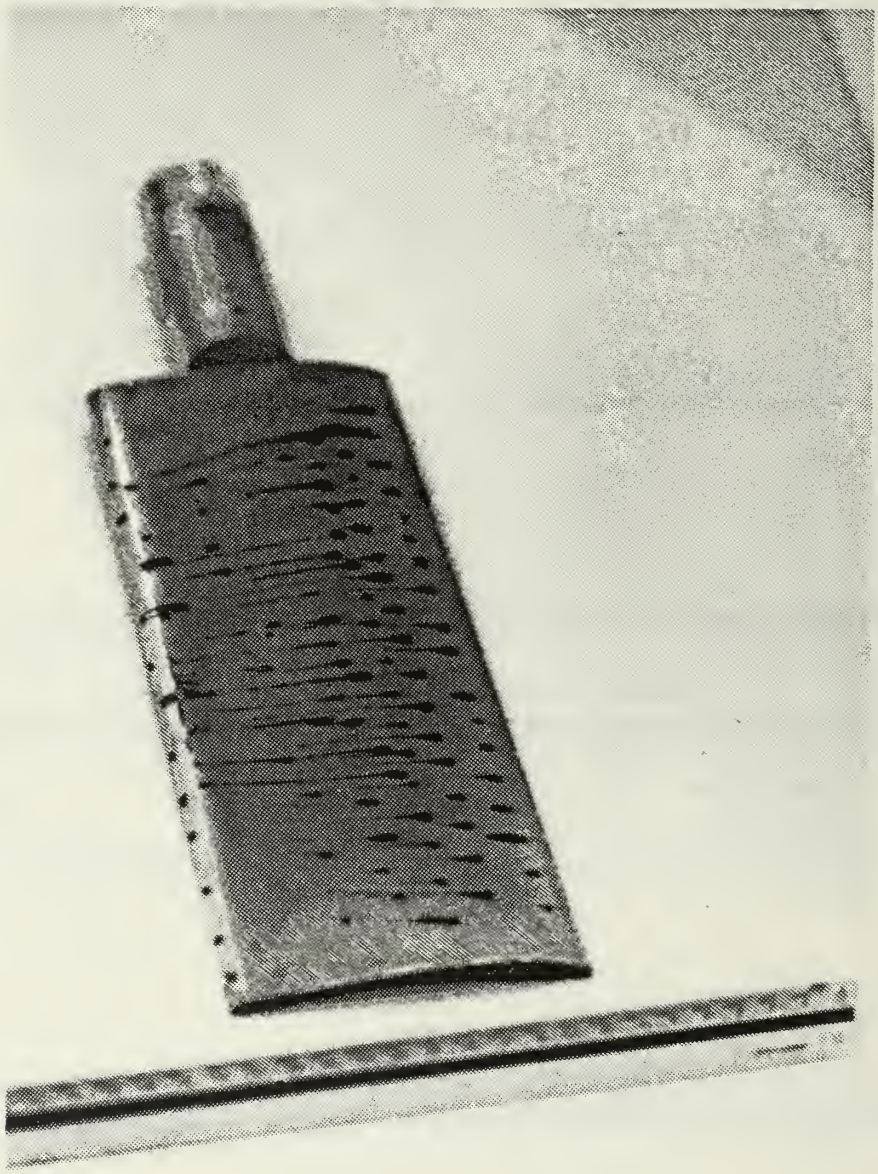

Figure 11. Surface flow pattern, suction surface at $\beta_1 = 68^{o}$.

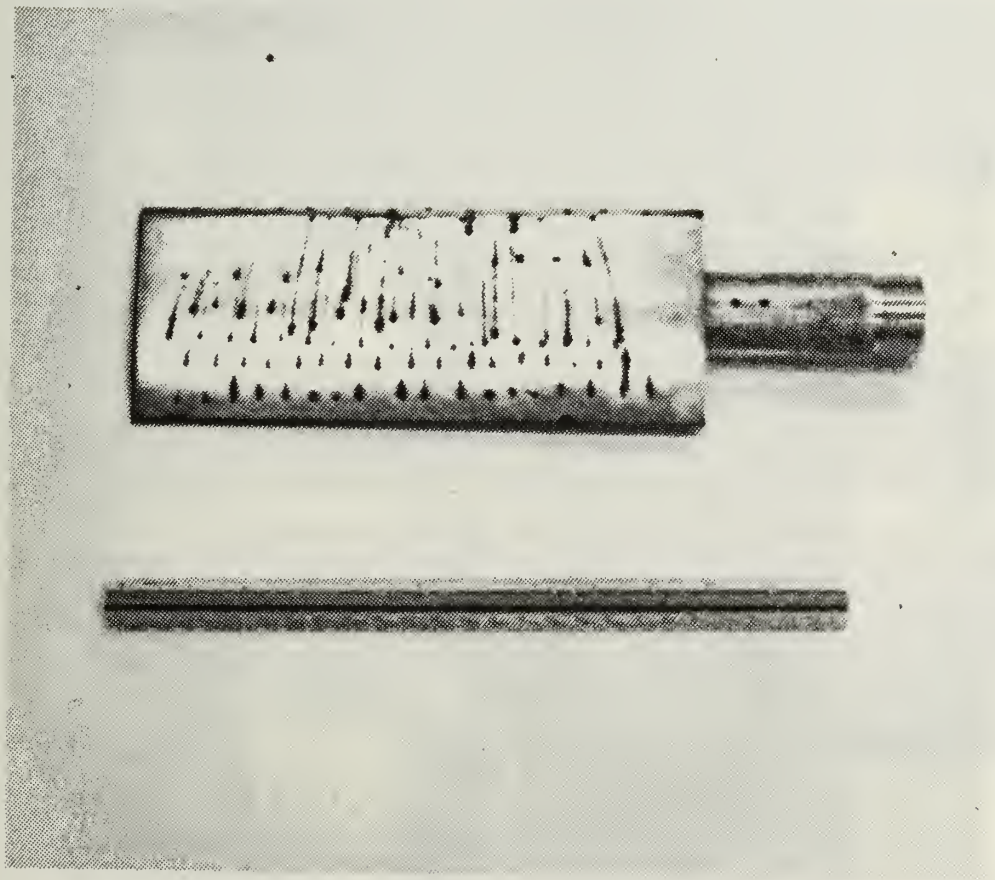

Figure 11(cont). Surface flow pattern, suction surface at $\beta_1 = 68^{\circ}$.

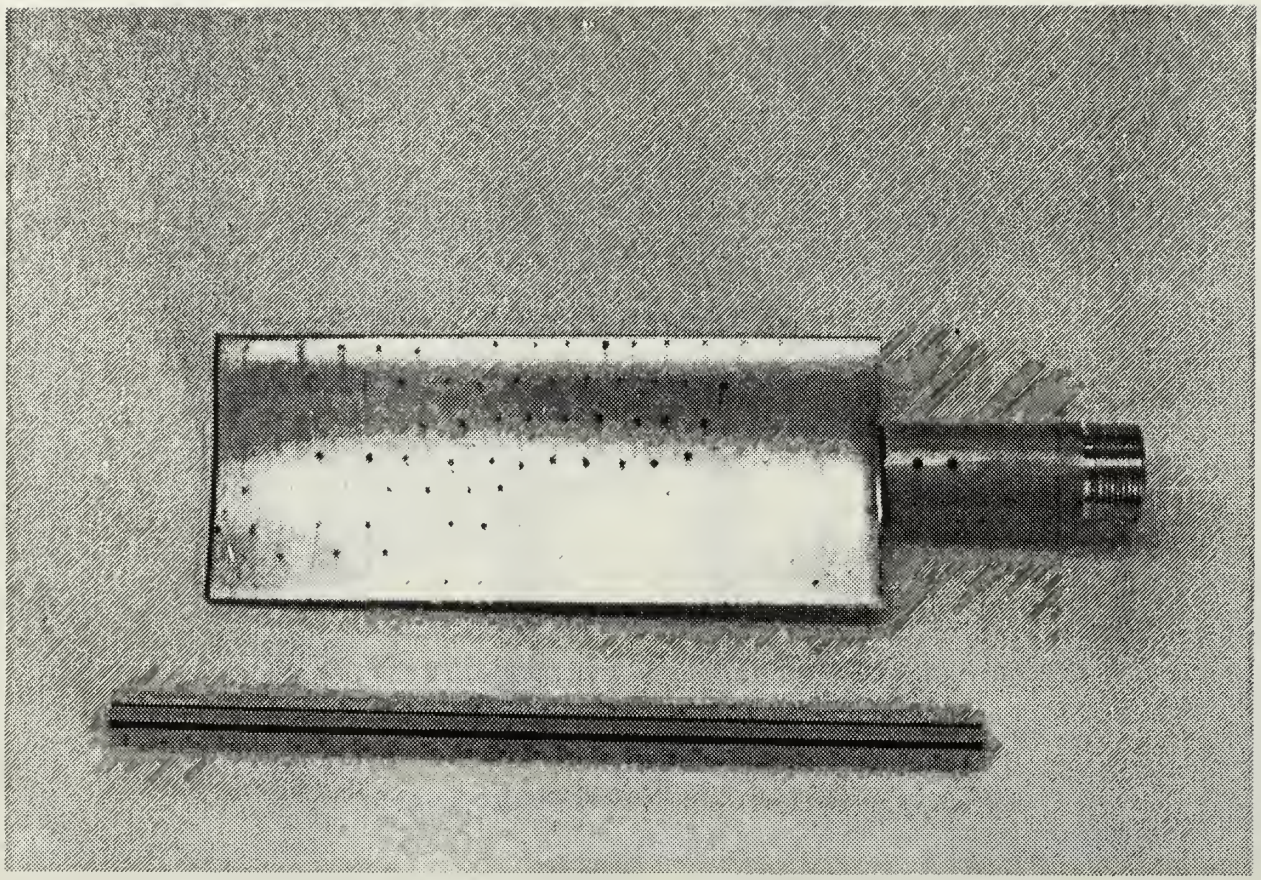

Figure 12. Surface flow pattern, pressure surface, $\beta_1 = 68^{o}$.

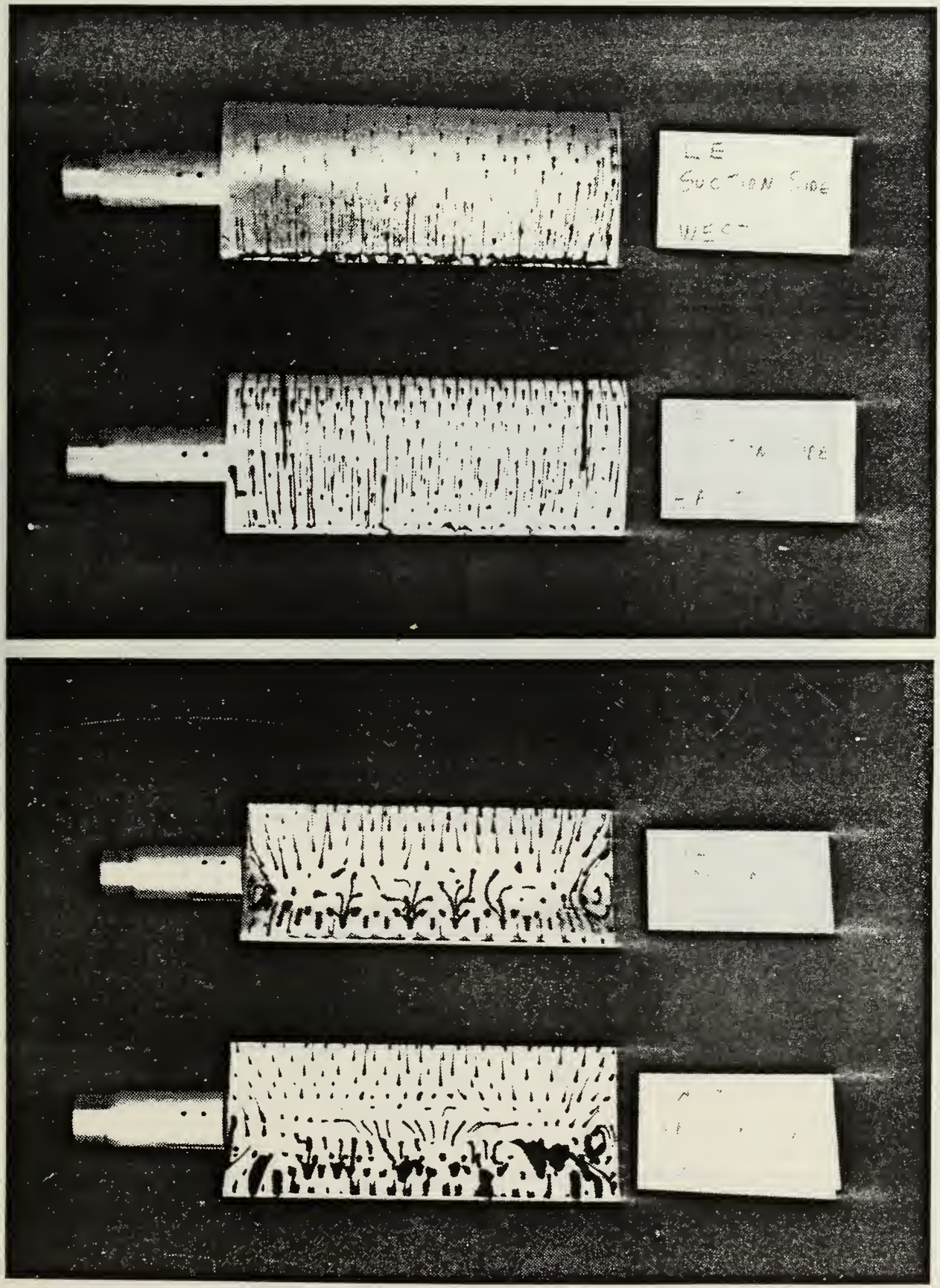

Figure 13. Surface flow patterns, $\beta_1 = 64^{\circ}$.

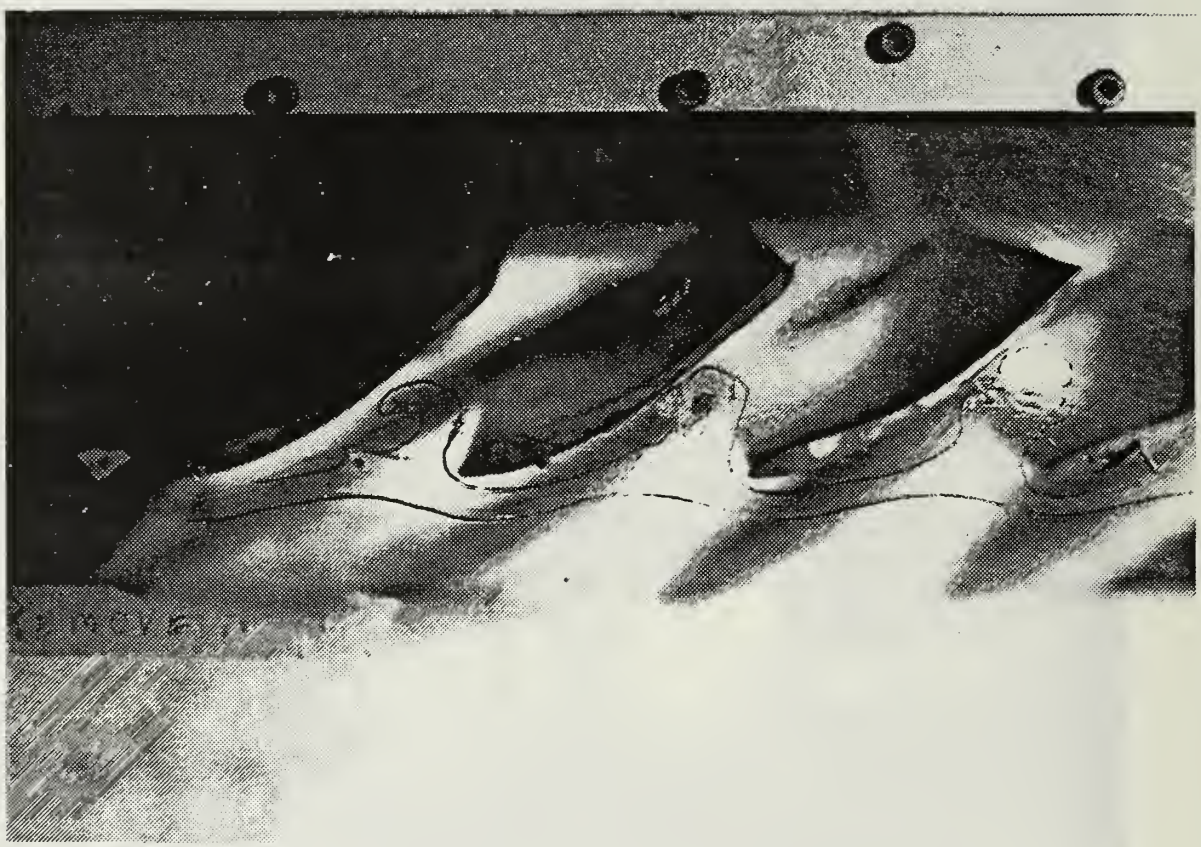

Figure 14. Surface flow along the wall.

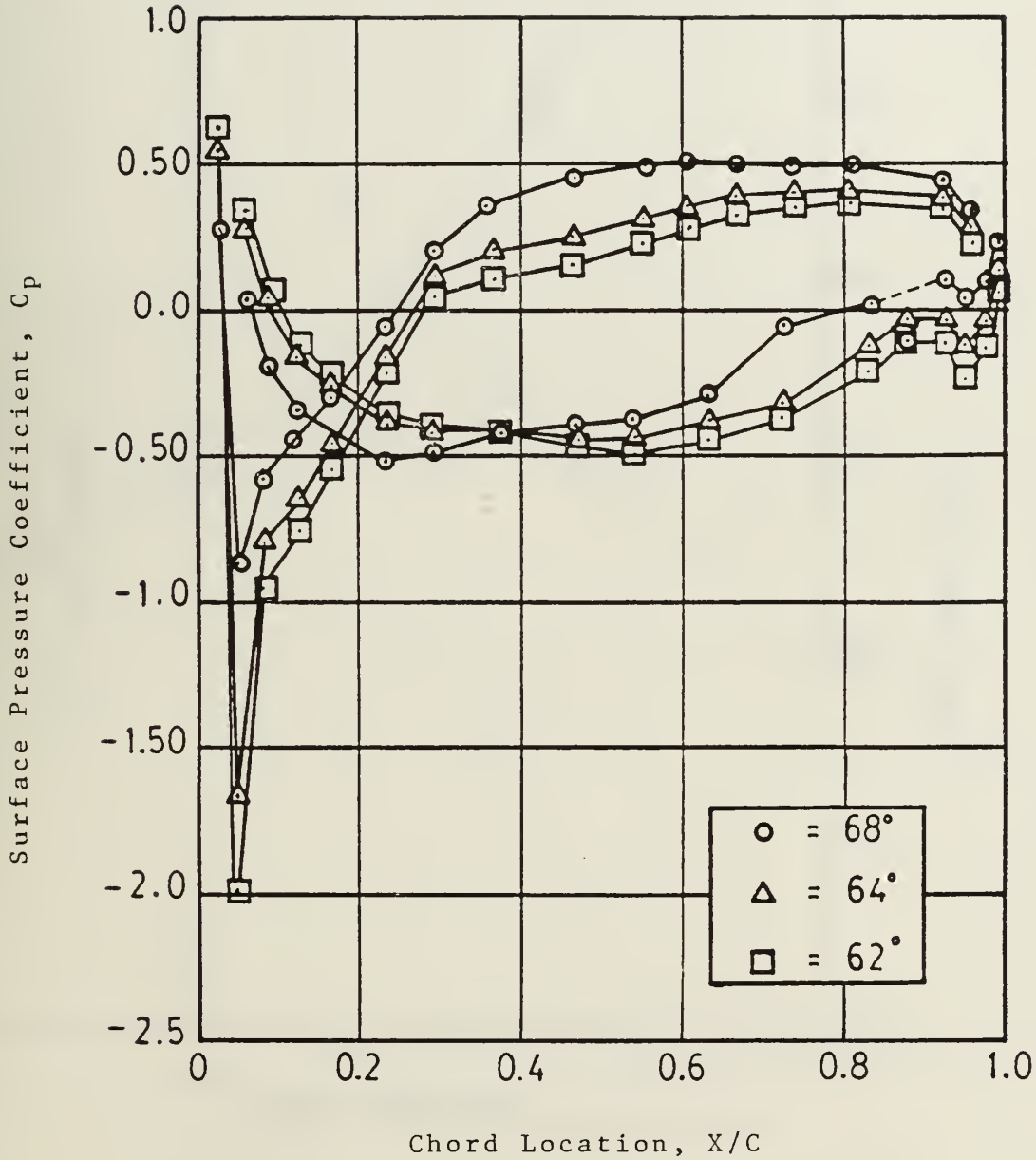

Figure 15. Surface Pressure Coefficient vs. Chordwise Location.

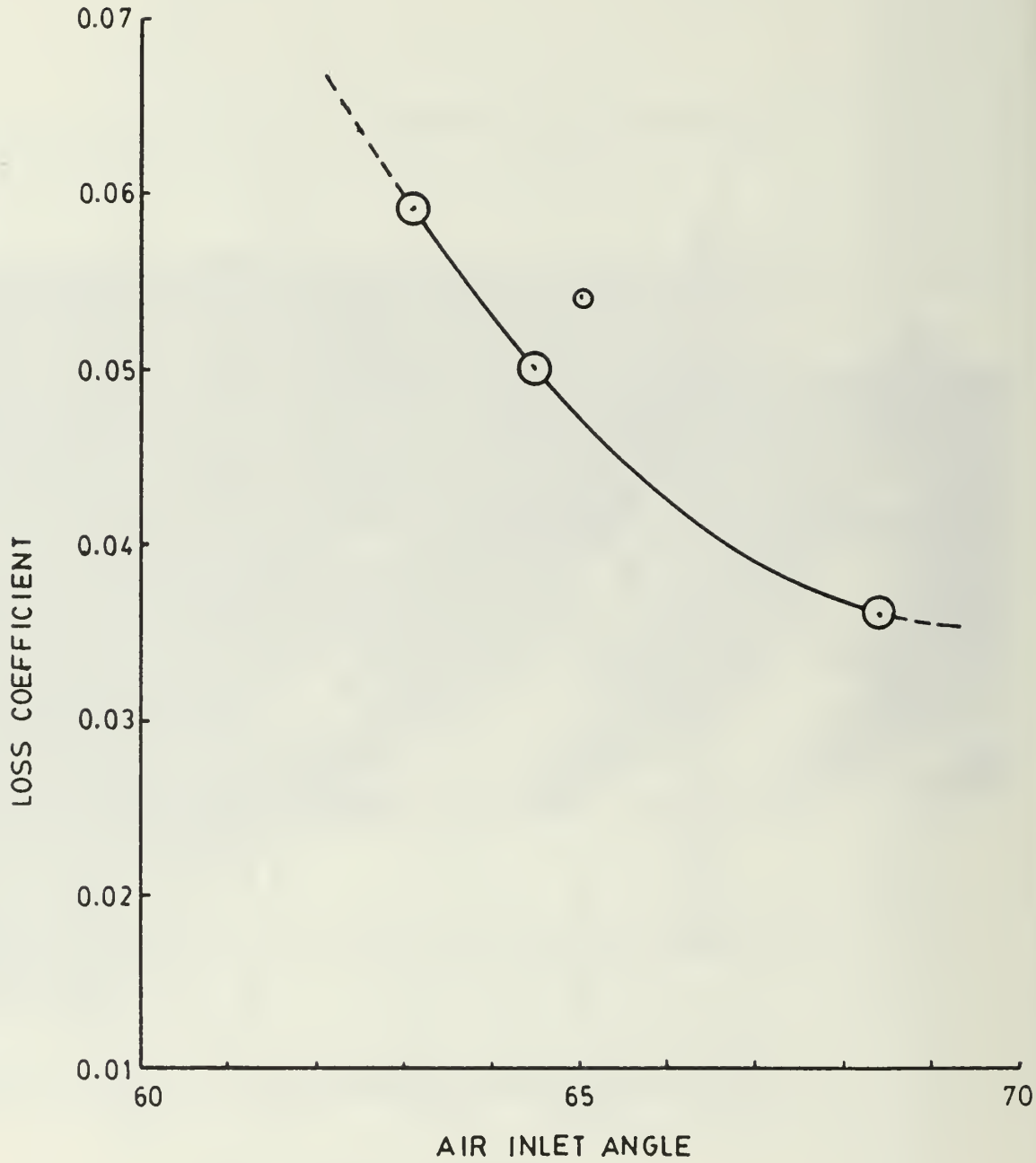

Figure 16. Loss coefficient vs. Air Inlet Angle.

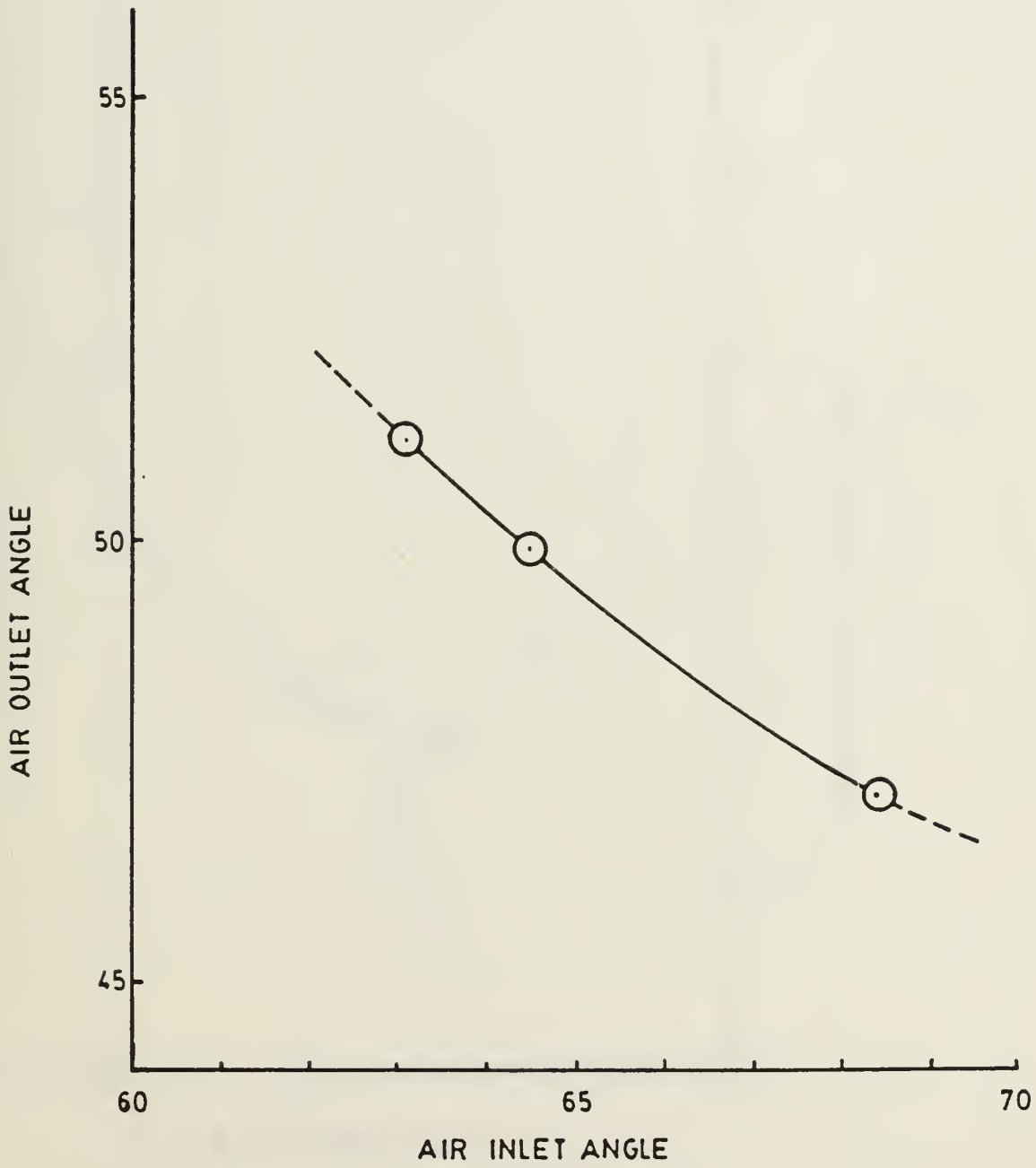

Figure 17. Air Outlet Angle vs. Air Inlet Angle.

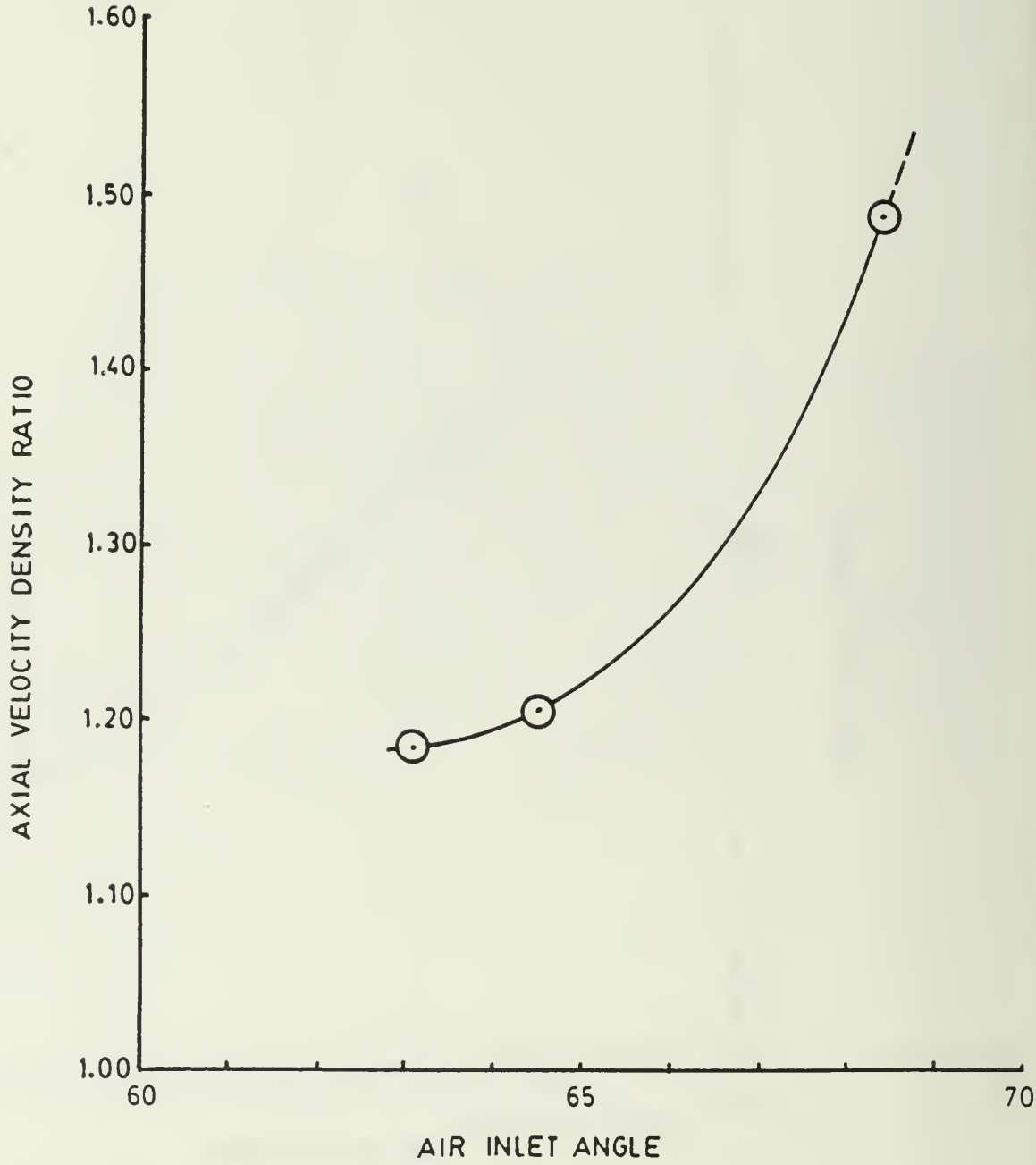

Figure 18. AVDR vs. Air Inlet Angle.

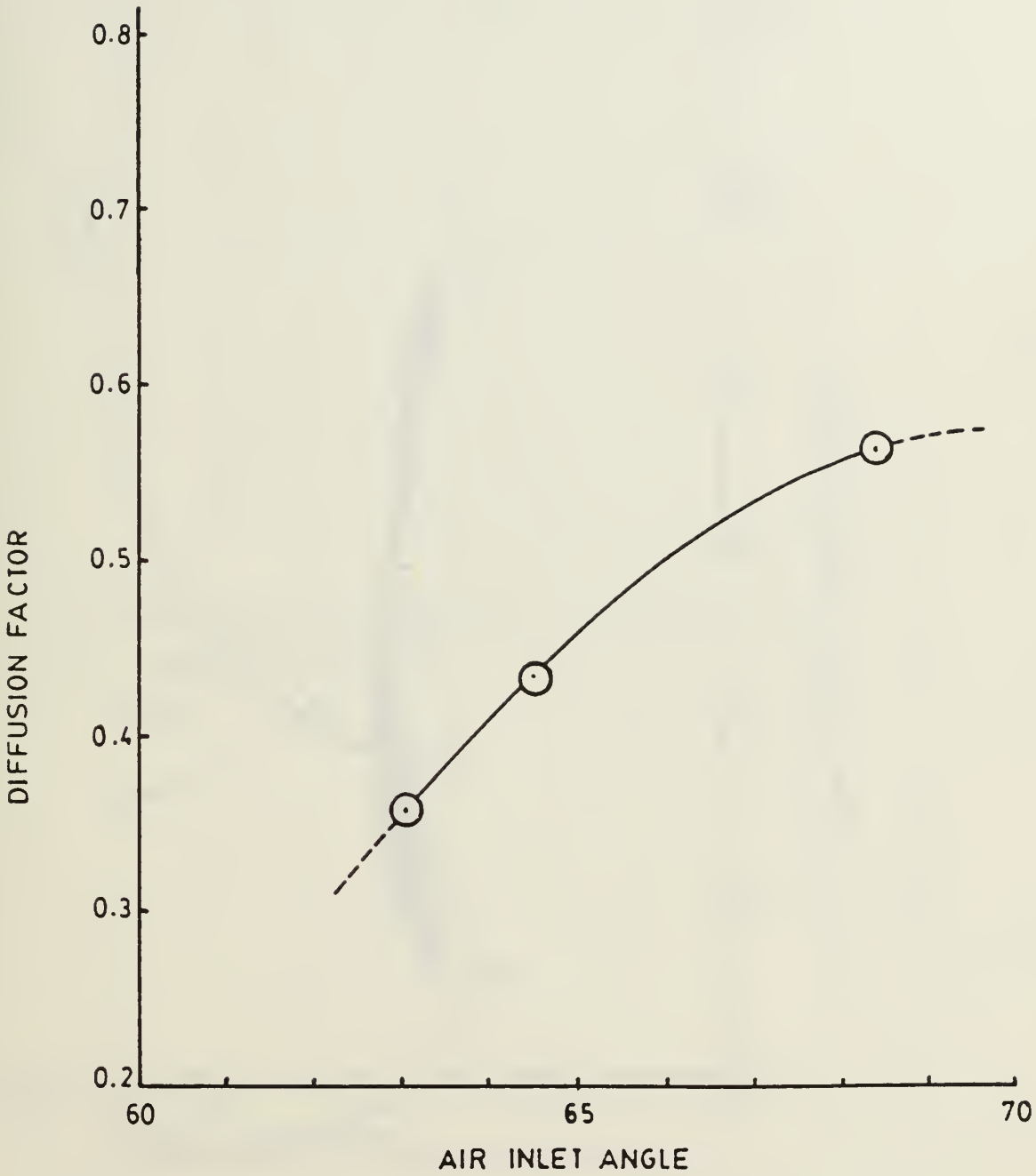

Figure 19. Diffusion Factor vs. Air Inlet Angle.

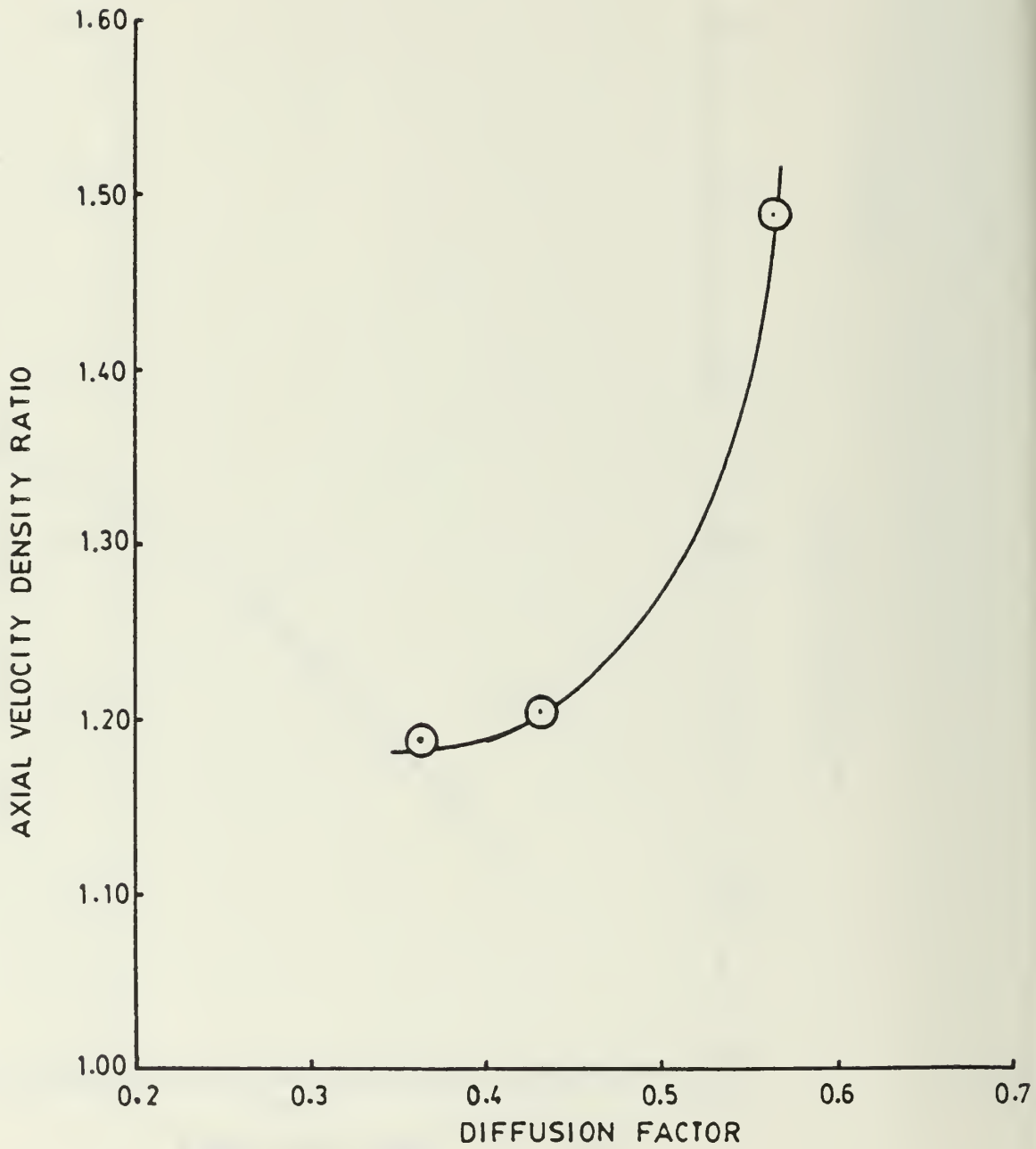

Figure 20. AVDR vs. Diffusion Factor.

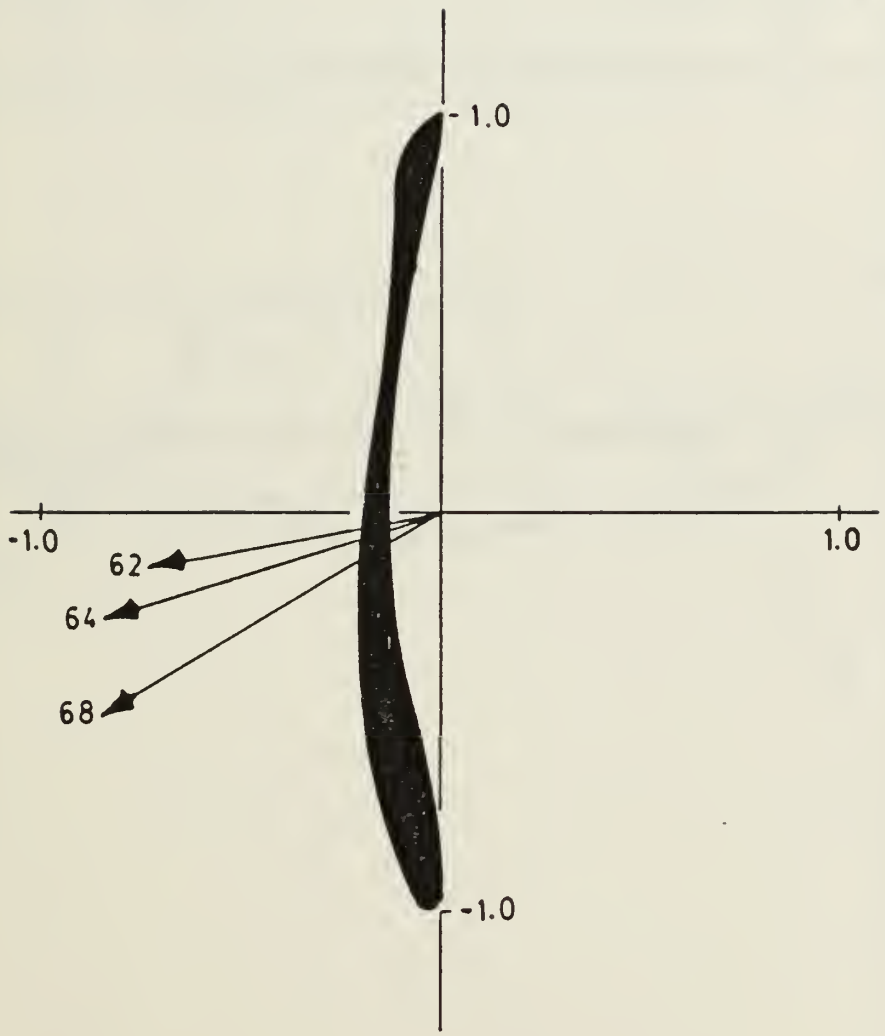

Figure 21. Blade Force Vectors.

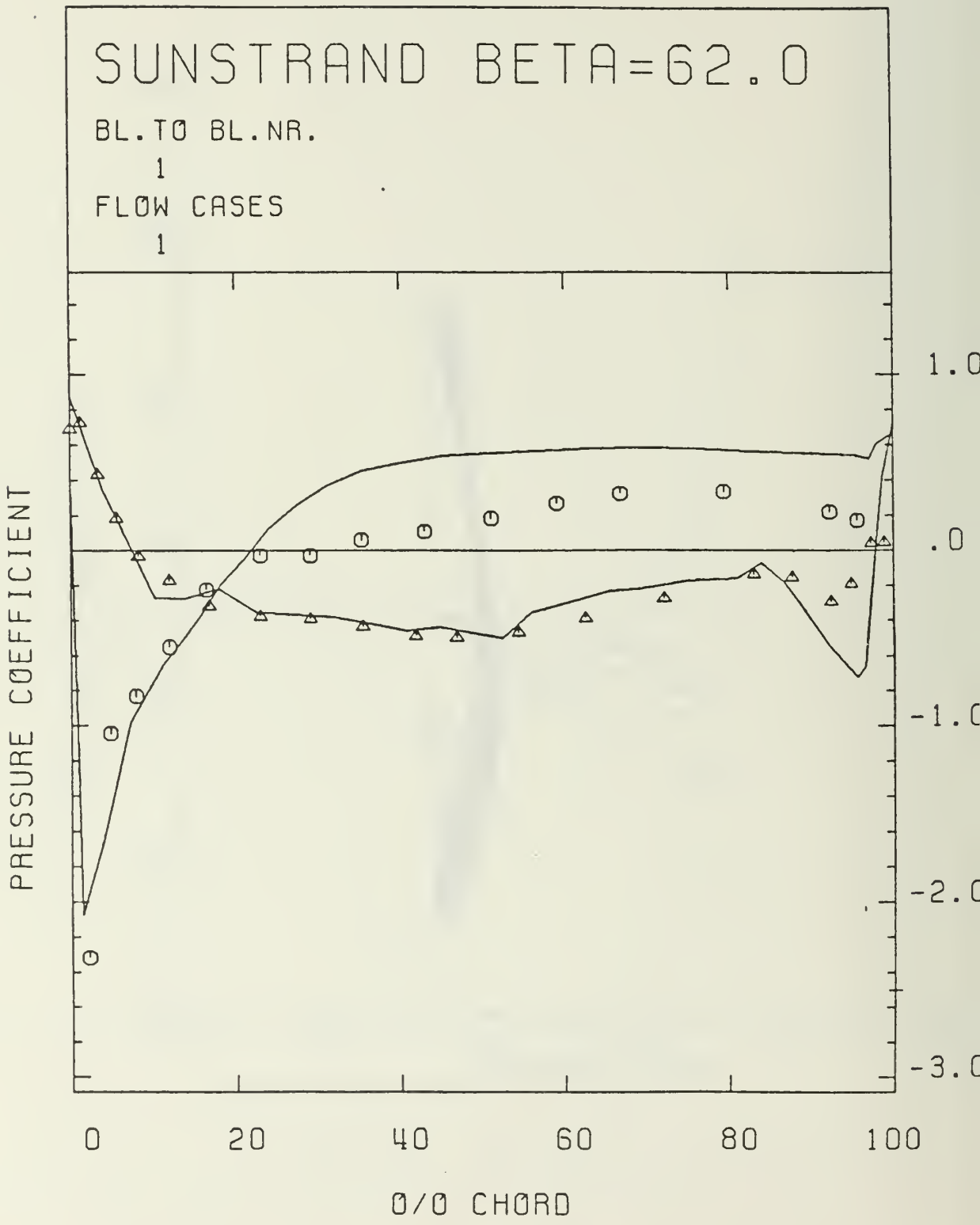

Figure 22(a). Blade Surface Static Pressure Distribution at $\beta_1 = 62^{\circ}$. (—— Q3DFLO-81 program; ○ pressure surface measurement, △ suction surface measurement)

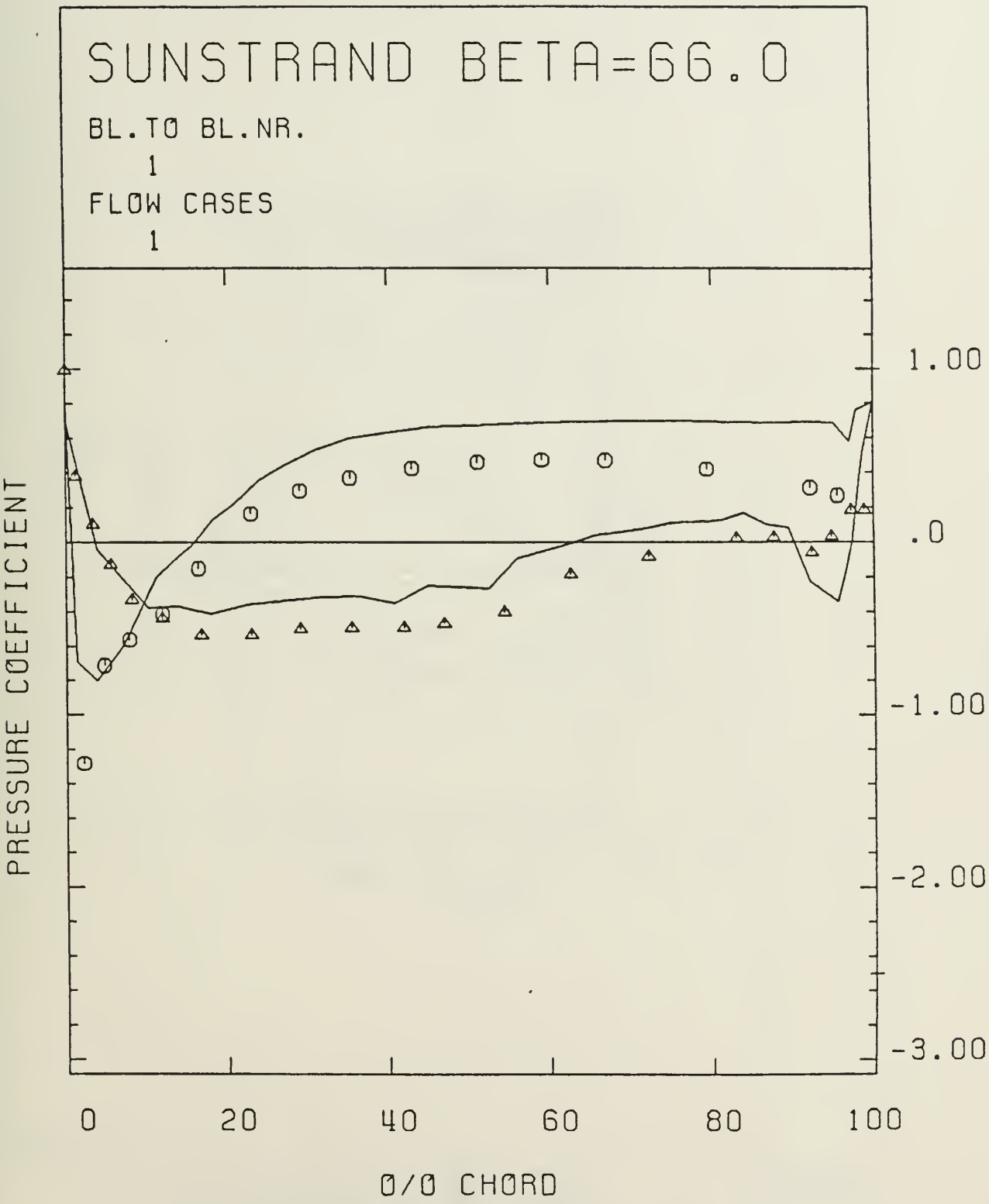

Figure 22(b). Blade Surface Static Pressure Distribution at β_1=66°. (—— Q3DFLO-81 program; ⊙ pressure surface measurement, △ suction surface measurement)

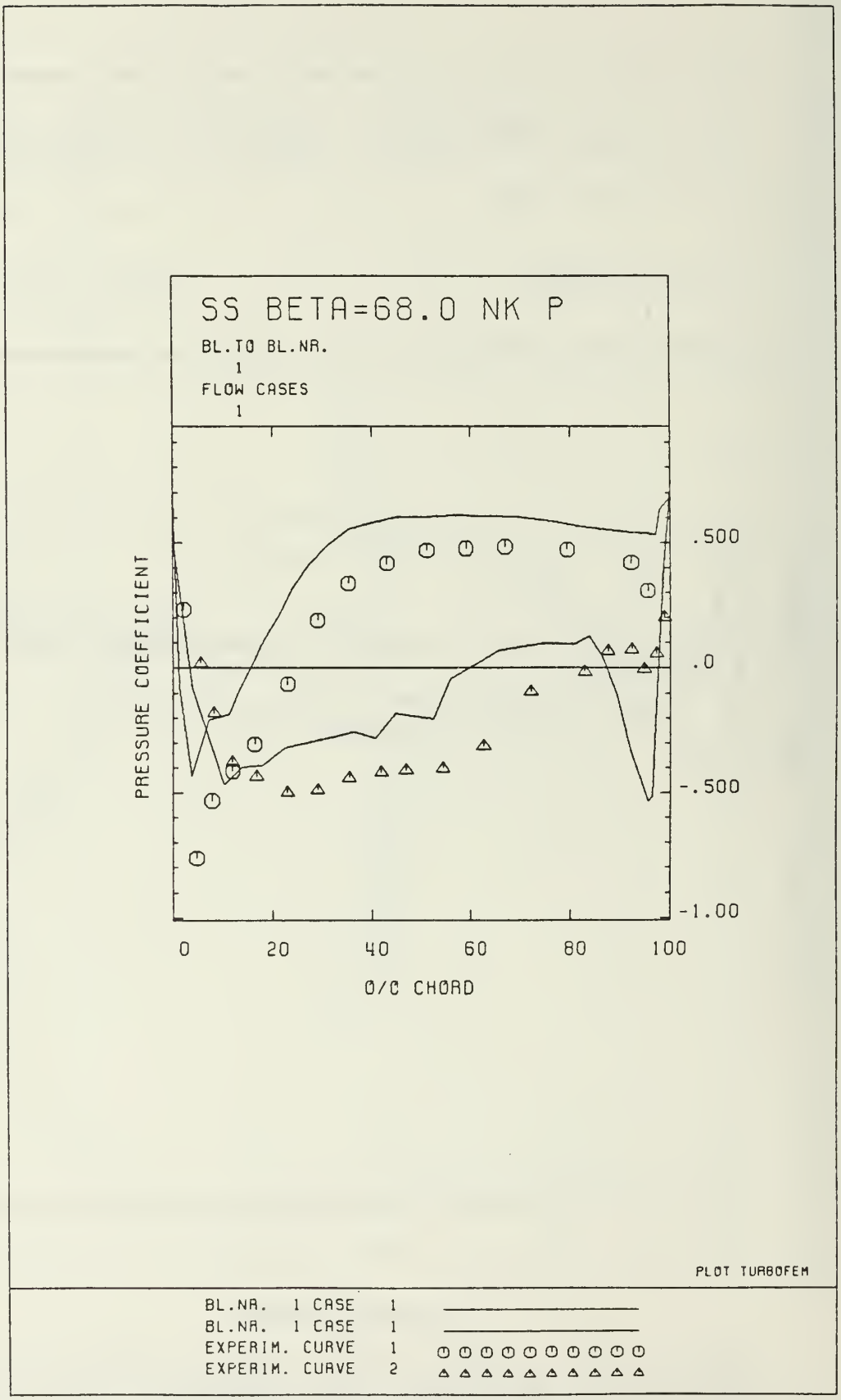

Figure 23(a). Blade Surface Static Pressure Distribution, at β_1=68°. (—— Q3DFLO-81 program; ⊙ pressure surface measurement, △ suction surface measurement)

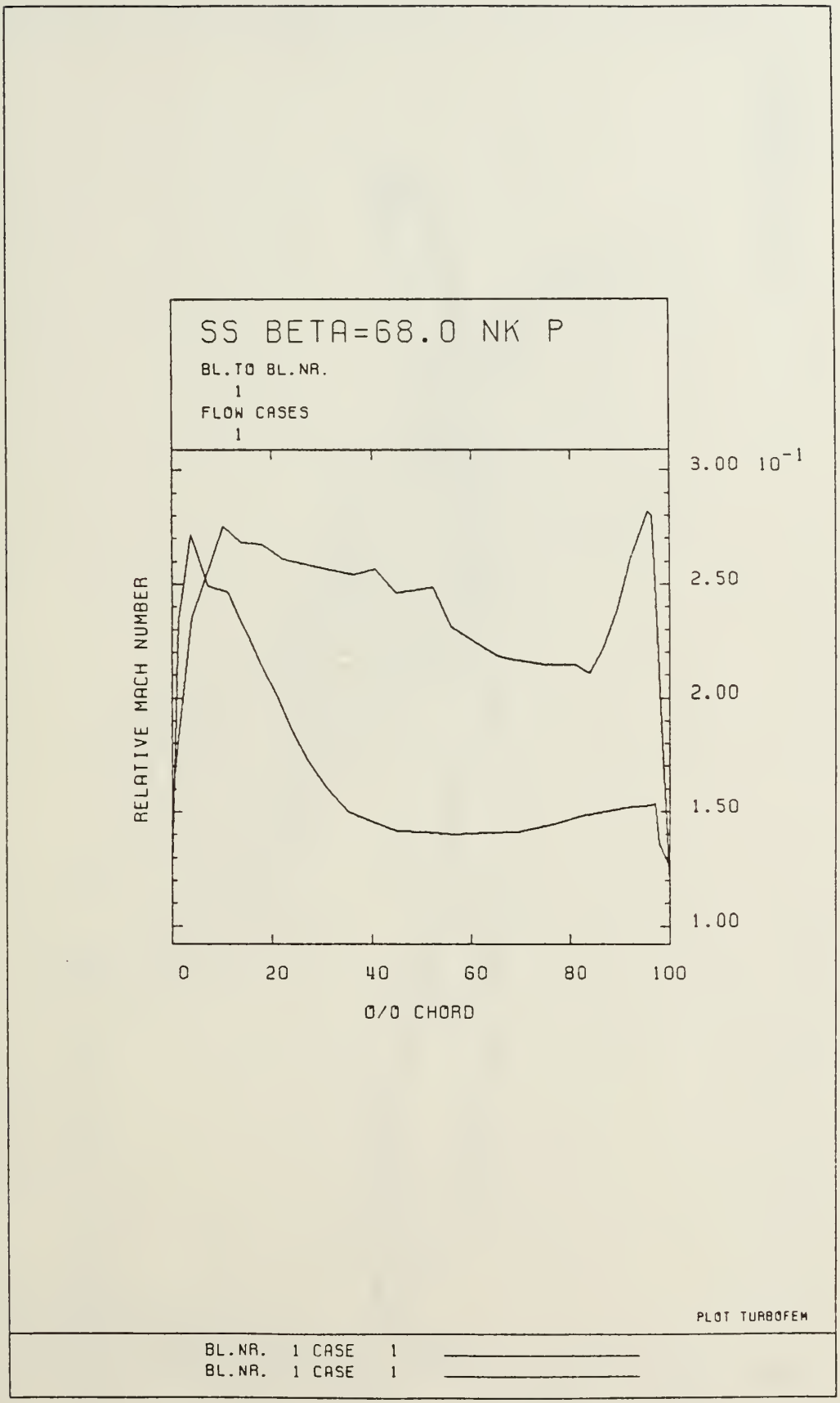

Figure 23(b). Blade Surface Mach Number Distribution at $\beta_1 = 68^{\circ}$ using Q3DFLO-81 Program.

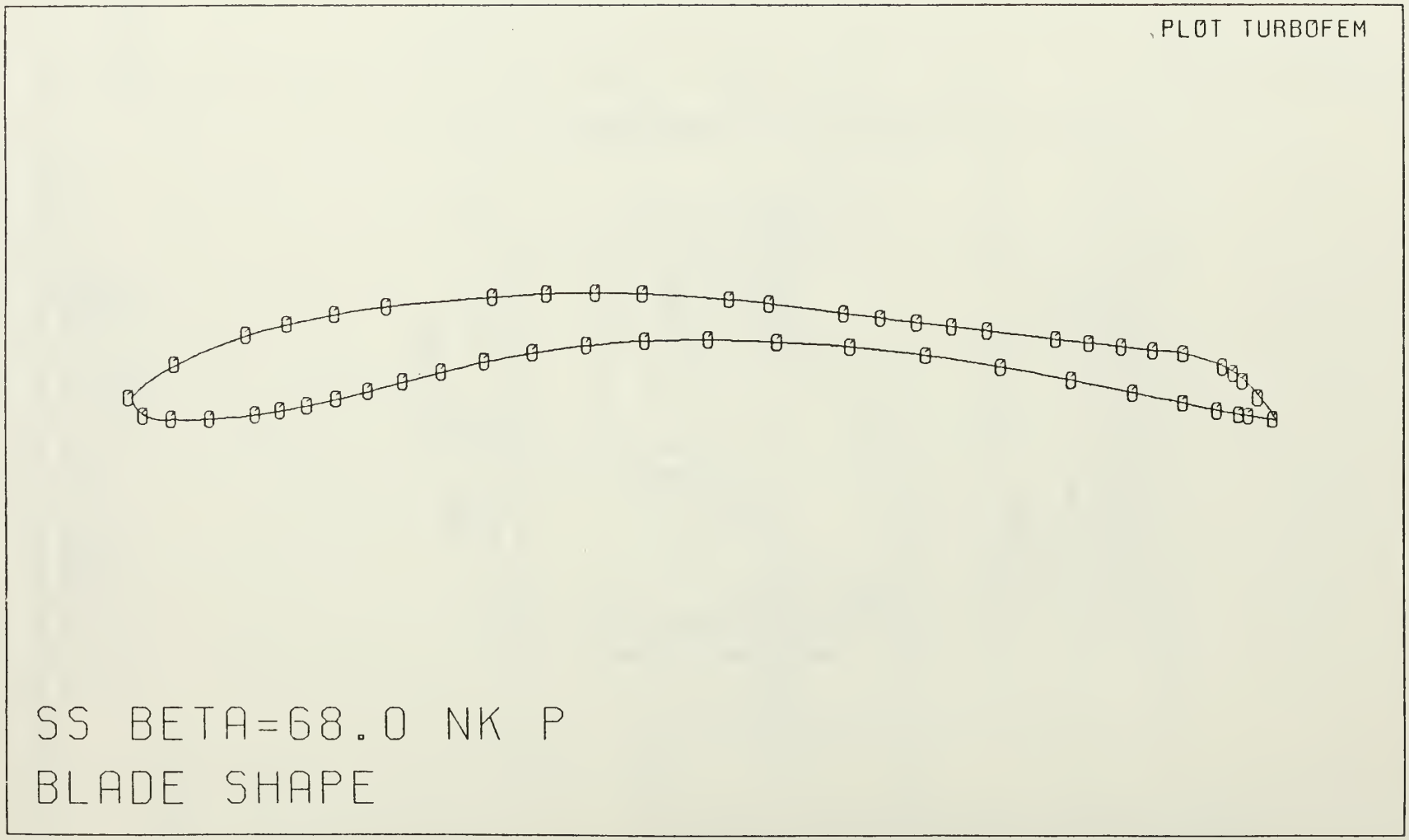

Figure 23(c). Surface Points for Q3DFLO-81 Mesh Generation.

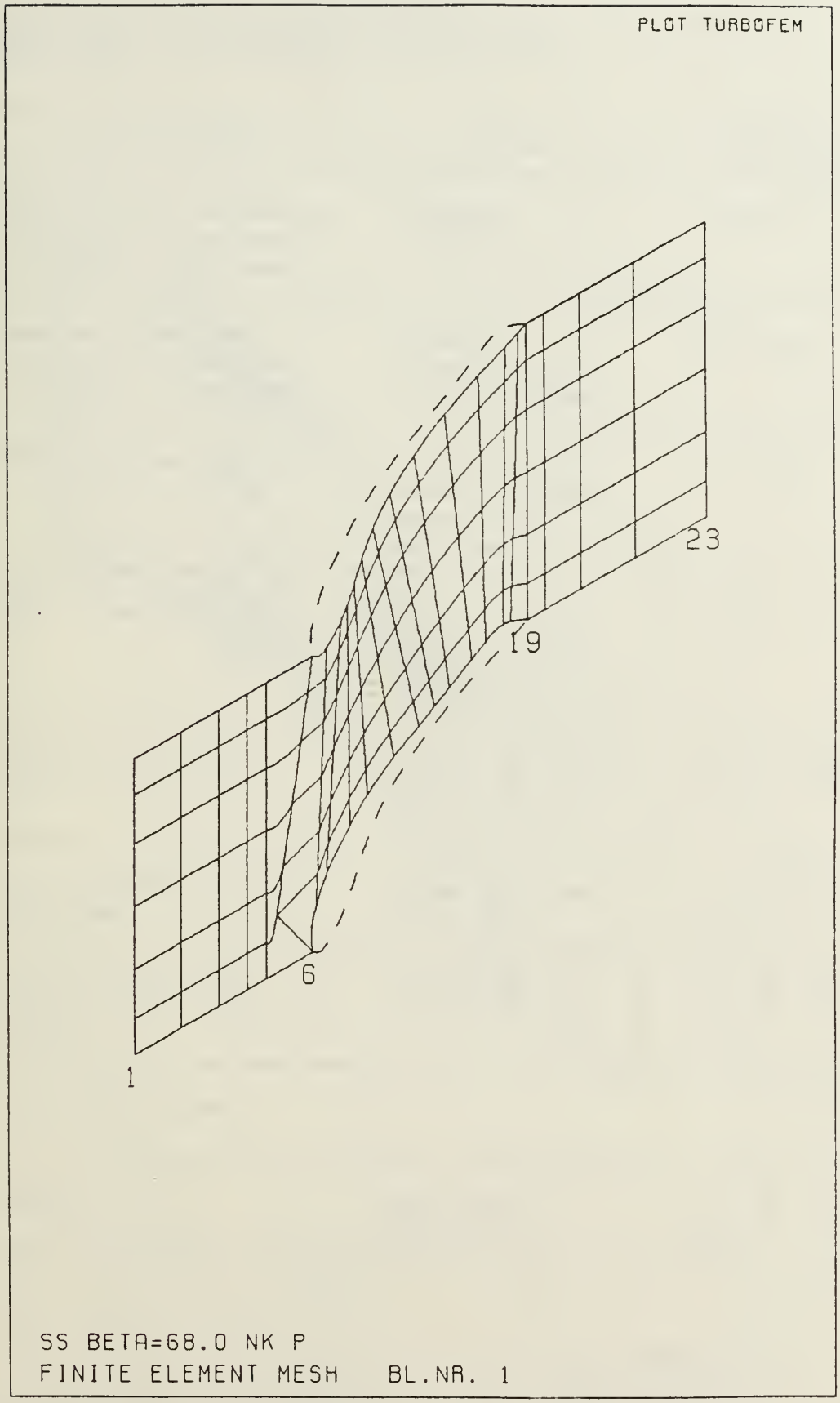

Figure 23(d). Q3FLO-81 Finite Element Mesh.

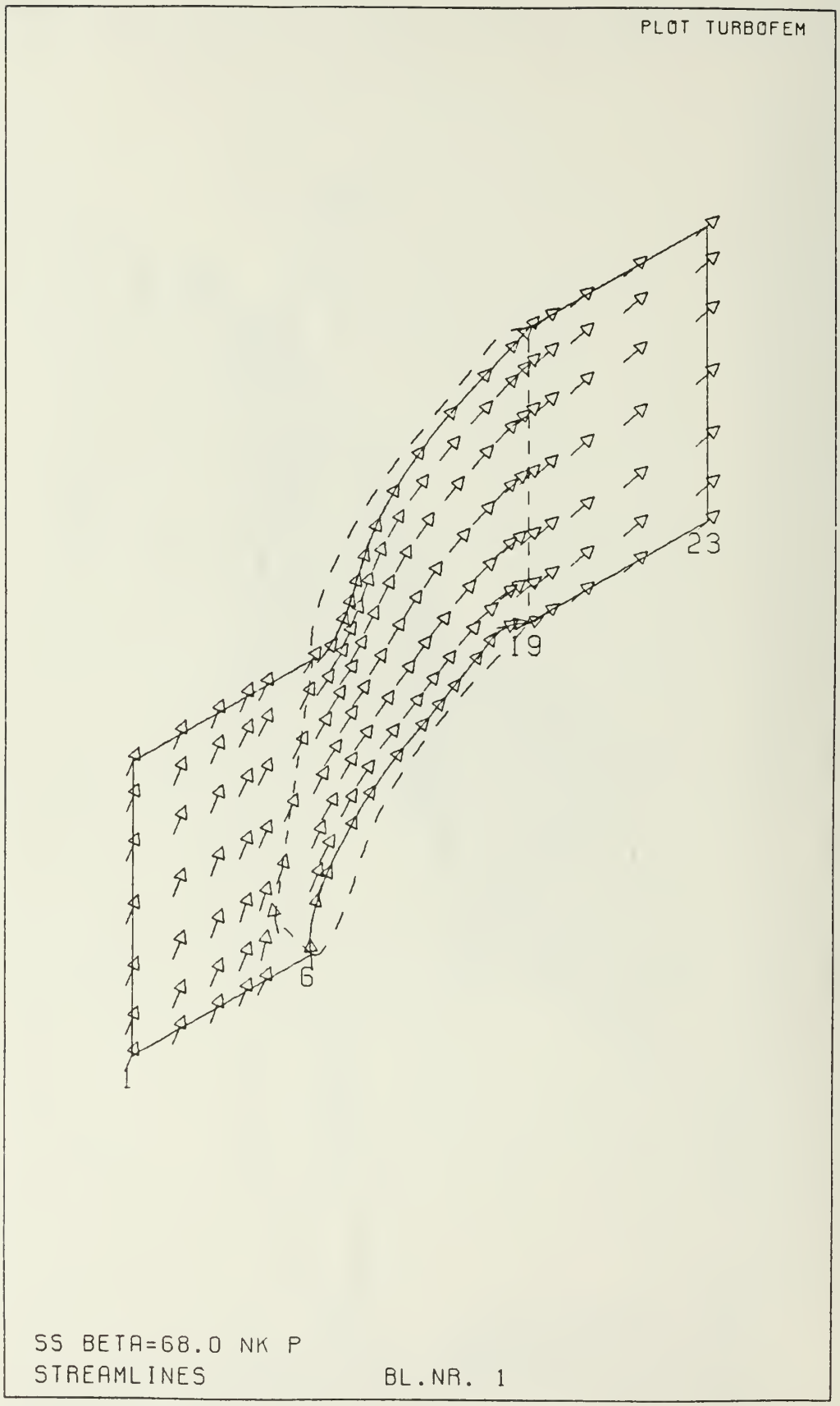

Figure 23(e). Streamlines at $\beta_1 = 68^\circ$ Using Q3DFLO-81 Program.

APPENDIX A.

MEASUREMENT UNCERTAINTY

Item	Description	Method	Uncertainty
x	Blade-to-Blade dimension x = 0 in. West end x = 60 in. East end	Position Potentiometer	±.01 in.
z	Spanwise dimension z = 0 in. North wall z = 10 in. South wall	Position Potentiometer on probe mount	±.01 in.
β_1	Inlet flow yaw angle	Angle Potentiometer on probe mount (hand adjustment)	±.2 deg.
β_2	Outlet flow yaw angle	Angle Potentiometer on probe mount (motor driven adjustment)	±.5 deg.
P_{plen}	Plenum total pressure	Static tap in plenum chamber V = 0	±.01 in. H_2O gauge
P_s	Static pressure at the test plane	Calibrated pneumatic probe	±.1 in. H_2O gauge
P_{wl}	Static pressure at x = 0 in., y = -16.25 in., z = 0 in.	Static tap on North wall	±.01 in. H_2O gauge
P_{ATM}	Atmospheric pressure		
P	Pressure	Scanivalve Transducer	±.01 in. H_2O gauge

APPENDIX B.

CASCADE PERFORMANCE FORMULAE

Parameter	General Expression	Programmed Expression
Loss Coefficient $\overline{\omega}$	(Note 1) $(\bar{C}p_{t_1} - \bar{C}p_{t_2})/(\bar{C}p_{t_1} - \bar{C}p_{1})$	(Note 2) $\dfrac{\int_o^s Cp_{t_1}\, k_1\, dx - \frac{1}{AVDR}\int_o^s Cp_{t_2}\, k_2\, dx}{\int_o^s Cp_{t_1}\, k_1\, dx - \int_o^s Cp_1\, k_1\, dx}$
Diffusion Factor D	$1 - \dfrac{W_2}{W_1} + \dfrac{\Delta W_u}{2\sigma W_1}$	$1 - \dfrac{\cos\bar{\beta}_1}{\cos\bar{\beta}_2} + \dfrac{\cos\bar{\beta}_1(\tan\bar{\beta}_1 - AVDR(\tan\bar{\beta}_2))}{(1 + AVDR)\sigma}$
Axial Velocity Density Ratio AVDR	h_1/h_2	(Note 2) $\dfrac{\int_o^s \left(\frac{Pt_2}{Pt_{ref}}\right)\left(\frac{X_2}{X_{ref}}\right)\left(\frac{1-X_2^2}{1-X_{ref}^2}\right)^{\frac{\gamma}{\gamma-1}} \cos\beta_2\, dx}{\int_o^s \left(\frac{Pt_1}{Pt_{ref}}\right)\left(\frac{X_1}{X_{ref}}\right)\left(\frac{1-X_1^2}{1-X_{ref}^2}\right)^{\frac{\gamma}{\gamma-1}} \cos\beta_1\, dx}$
Static Pressure Rise Coefficient Cp_{static}	$\dfrac{\bar{P}_2 - \bar{P}_1}{\bar{P}_{t_1} - \bar{P}_1}$	$\dfrac{\frac{1}{AVDR}\int_o^s Cp_2\, k_2 dx - \int_o^s Cp_1\, k_1\, dx}{\int_o^s Cp_{t_1}\, k_1 dx - \int_o^s Cp_1\, k_1\, dx}$

Loss Coefficient Parameter Ω	$\frac{\bar{\omega}\cos^3\beta_2}{2\sigma\cos^2\beta_1}$	$\frac{\omega\cos^3\bar{\beta}_2}{2\sigma\cos^2\bar{\beta}_1}$
Incidence Angle i	$\beta_1 - \gamma - \phi/2$	$\bar{\beta}_1 - \gamma - \phi/2$
Deviation Angle δ	$\phi/2 - \gamma + \beta_2$	$\phi/2 - \gamma + \bar{\beta}_2$

Note 1: "Barred" quantities are average values computed over a selected integration interval--usually one blade space.

Note 2: Derivation of programmed expression is given in Reference 1.

APPENDIX C

NOTATIONS

ADVR	Axial Velocity--Density Ratio
C_{fB}	Coefficient of force based on surface pressure integration
C_{fM}	Coefficient of force based on momentum conservation
$C_{p_{static}}$	Coefficient of static pressure rise
C_{xB}	Coefficient of force in the x direction based on blade surface pressure integration
C_{yB}	Coefficient of force in the y direction based on blade surface pressure integration
C_{xM}	Coefficient of force in the x direction based on momentum conservation
C_{yM}	Coefficient of force in the y direction based on momentum conservation
c	Blade chord (inches)
D	Diffusion factor
h_i	Spanwise depth of control volume at inlet (i = 1) or outlet (i = 2)
i	Incidence angle (degrees)
k_1	$[\int_o^s \rho_1 V_1 \cos\beta_1 dx]/[\int_o^s \rho_{ref} V_{ref} \cos\beta_1 dx]$
k_2	$[\int_o^s \rho_2 V_2 \cos\beta_2 dx]/[\int_o^s \rho_{ref} V_{ref} \cos\beta_2 dx]$
P	Pressure (in H_2O)
Q	Dynamic Pressure (in H_2O)
s	Blade-to-blade spacing (inches)
T	Temperature (°R)

V	Velocity (ft/sec)
W	Relative velocity (ft/sec)
X	Velocity, non-dimensionalized by the "limiting" velocity, $V_T = \sqrt{2 C_p T_t}$
x	Coordinate in the axial direction (inches)
z	Coordinate in the spanwise direction (inches)
β	Air angle, measured in the blade-to-blade plane (degrees)
γ	Stagger angle (degrees)
δ	Deviation angle (degrees)
σ	Solidity (c/s)
Φ	Pitch angle (of air flow), measured in the spanwise, blade-to-blade plane
ϕ	Blade camber angle (degrees)
Ω	$[\bar{\omega}\cos^3\beta_2/2\sigma\cos^2\beta_1]$ Loss coefficient parameter
$\bar{\omega}$	Loss coefficient

Subscripts

i	Refers to traversing plane; i = 1 for inlet, i = 2 for outlet
p	Pressure
plen	Plenum (supply)
s	Static
t	Total
u	In the blade-to-blade (x) direction
wℓ	North wall, lower plane
1	Inlet plane
2	Outlet plane

References

1. Koyuncu, Y "Report of Tests of a Compressor Configuration of CD Blading", Naval Postgraduate School M. S. Thesis, March 1984.

2. Cina, F. S. "Subsonic Cascade Wind Tunnel Tests Using a Compressor Configuration of DCA Blades", Naval Postgraduate School Masters Thesis, June 1981.

3. Himes, S. J. "Report of Tests of a Compressor Configuration of DCA Blading", Naval Postgraduate School Masters Thesis, June 1983.

4. Hirsch, Ch. and Warzee, G. "An Integral Quasi-3D Finite Element Calculation Program for Turbomachinery Flow", ASME Journal of Engineering for Power, Vol 101, pp 141-148, January 1979.

DISTRIBUTION LIST

1.	SUNDSTRAND Operations (Attn: Paul Hermann) Advanced Technology Group Sundstrand Corporation 4747 Harrison Av. Rockford, IL 61101	8
2.	Naval Postgraduate School Monterey, CA 93943	
	Attn: Research Administration (012)	1
	Turbopropulsion Laboratory (67Sf)	7